CHAPTER 3

CHARACTERIZATION OF CRYSTALLINE PHASES

3.1 Introduction

Solid substances form when the electrostatic interactions between atoms, ions, or molecules overcome thermal motion and cause the loss of translational freedom *[26]*. The spatial arrangements that the species settle into depend on the nature of the bonding forces present, but will always represent a configuration that minimizes the electrostatic interactions or lattice energy *[26]*.

Different types of chemical bonding cause solids to be organized in specific manners. Materials like silicates and metal oxides are composed of atoms that display both ionic and covalent character in their bonding. These materials usually form chains that extend through the entire crystal, so that a large variety of stable periodic crystalline arrangements can be expected in such materials *[26]*.

Amorphous materials belong to a category of solids whose packing arrangements do not have any long-range periodicity. In amorphous solids, the atomic

arrangements also correspond to a minimum packing energy, albeit one of higher energy than the thermodynamically stable crystalline phase, at a given temperature and pressure *[26]*.

One important difference between crystalline and amorphous materials is in how they scatter an X-ray beam. Crystalline forms produce sharp lines due to diffraction of the X-ray beam, whereas amorphous forms only produce few broad peaks due to some short-range order in the atomic arrangement. The properties of the lines produced by X-ray diffraction of crystalline solids strongly depend on the properties of the crystalline solid *[26]*. X-ray diffraction is therefore very well suited for the characterization of the crystalline phases that formed in the prepared samples.

3.2 Background on X-ray Powder Diffraction

3.2.1 Diffraction of X-rays and Bragg's Law

When a periodic array of objects each scatter radiation coherently, the concerted constructive interference at specific angles is called diffraction. The atoms in a crystal are in a periodic array. As the distances between the atoms in a crystal are in the order of angstroms, interference effects will therefore be seen if the incident wave front also has a wavelength in the order of angstroms, i.e. in the X-ray region of the spectrum (visible light will not be diffracted by the atoms in a crystal).

A crystal has many three-dimensional periodic relationships between the atoms that compose it, so that a crystal may diffract a monochromatic wave in a number of different directions in three-dimensional space. The angles of this diffraction will only depend on the various periodic relationships between the atoms composing the crystal *[26, 27]*.

Consider Figure 3.1. The X-ray beams are incoming from the left and are reflecting from each of the planes. If the initial waves are in phase with one another and the waves reflect from each plane, the controlling equation can be derived as follows: for reflection, the angle of incidence (θ) must equal the angle of reflection (θ'). The wave reflecting from the second plane must travel a distance ABC further than

the wave reflecting from the top plane. Thus, all waves reflecting from the planes below the surface will be phase retarded with respect to the first wave, causing interference. When ABC is equal to the wavelength (λ), the reflection from all planes below the surface will be in phase and constructive interference (diffraction) will occur.

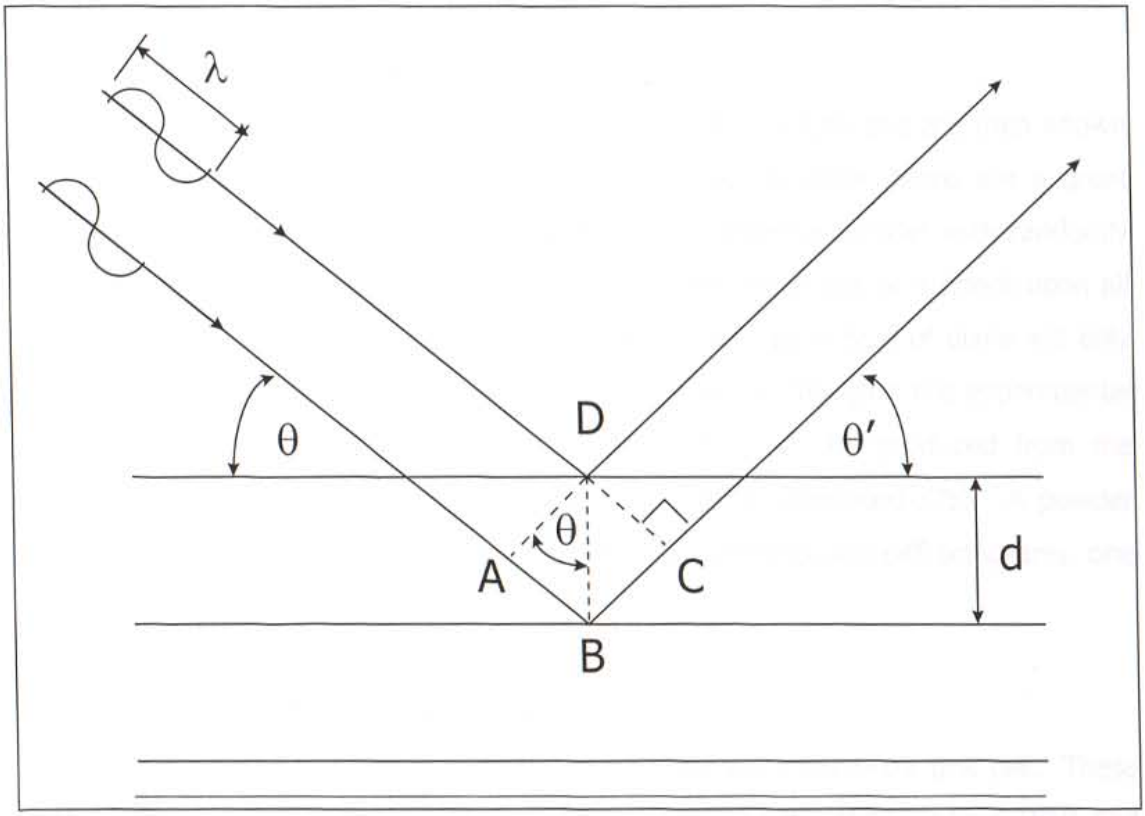

Figure 3.1: Bragg's law diagram

From figure 3.1, it can be seen that

$$\sin\theta = \frac{AB}{d} \tag{3.1}$$

When diffraction occurs,

$$ABC = 2AB = \lambda \tag{3.2}$$

By substituting Equation 3.2 into Equation 3.1, the well-known Bragg equation thus results:

$$n\lambda = 2d\sin\theta \tag{3.3}$$

where n = integer and λ is the X-ray wavelength.

A reinforced X-ray intensity will therefore occur in the vicinity of the crystal providing that both the incident and reflecting angles are equal and that the conditions for Equation 3.3 is met.

3.2.2 The Powder Diffraction Pattern

Powders very often consist of a great amount of tiny crystals and are then known as polycrystalline materials *[26]*. In polycrystalline materials, there are a great number of crystallites in all possible orientations. When a powder with randomly oriented crystallites is placed in an X-ray beam, the beam will be incident upon all possible interatomic planes. However, diffraction from each type of plane will only occur at its characteristic diffraction angle θ. Thus, by changing the experimental angle 2θ, all of the possible diffraction peaks that can be produced from the differently oriented crystallites in the powder, will be generated *[26]*. A powder diffraction pattern is thus made up of a series of superimposed diffractograms, one for each unique phase in the powder.

3.2.3 The Position of Diffraction Peaks

There are an infinite number of sets of planes that can intersect a unit cell. These sets of crystallographic planes may be described with the Miller indices (hkl) and their d_{hkl} interplanar spacings *[26, 27]*. The d_{hkl} values are a geometric function of the size and shape of the unit cell. The relationship between d_{hkl} and the real unit cell is cumbersome and usually stated in a different form for each crystal system. Taking the dot product of the vector d^*_{hkl}, it can be shown *[26]* that

$$d^*_{hkl}{}^2 = h^2\mathbf{a}^{*2} + k^2\mathbf{b}^2 + l^2\mathbf{c}^{*2} + 2hk\mathbf{a}^*\mathbf{b}^*\cos\gamma^* + 2hk\mathbf{a}^*\mathbf{c}^*\cos\beta^* + 2hk\mathbf{b}^*\mathbf{c}^*\cos\alpha^* \qquad (3.4)$$

where h, k and l are the Miller indices,

a, b and c are the edges of the unit cell and

α, β and γ are angles between c/b, c/a and a/b, respectively.

Descriptive data for crystal symmetry systems are given in Table 3.1 *[27]*. From

Equation 3.4 it can be seen that in the cubic symmetry system ($a = b = c, \alpha = \beta = \gamma = 90°$) the following relationship is valid:

$$d^*_{hkl}{}^2 = (h^2 + k^2 + l^2)\,\mathbf{a}^{*2} \tag{3.5}$$

In the tetragonal symmetry system the relationship is

$$d^*_{hkl}{}^2 = (h^2 + k^2)\,\mathbf{a}^{*2} + l^2\mathbf{c}^{*2} \tag{3.6}$$

In the hexagonal symmetry system the relationship is

$$d^*_{hkl}{}^2 = (h^2 + hk + k^2)\,\mathbf{a}^{*2} + l^2\mathbf{c}^{*2} \tag{3.7}$$

In the orthorhombic symmetry system the relationship is

$$d^*_{hkl}{}^2 = h^2\mathbf{a}^{*2} + k^2\mathbf{b}^2 + l^2\mathbf{c}^{*2} \tag{3.8}$$

Table 3.1: Descriptive data for crystal symmetry systems

Symmetry System	**Axial Ratios**	**Angles Between Crystal Axes**
triclinic	a:b:c	α, β, γ
monoclinic	a:b:c	β ($\alpha = \gamma = 90°$)
orthorhombic	a:b:c	all angles 90°
tetragonal	a:c (b = a)	all angles = 90°
hexagonal division		
hexagonal axes	a:c (b = a)	$\gamma = 120°$ ($\alpha = \beta = 90°$)
orthohexagonal	a:b:c ($b = a\sqrt{3}$)	all angles 90°
rhombohedral	a = b = c	$\alpha = \beta = \gamma \neq 90°$
cubic	a = b = c	$\alpha = \beta = \gamma = 90°$

Equation 3.4 permits the computation of all the possible d_{hkl} values for any unit cell *[26]*. Each of these d_{hkl} values fits into Bragg's law (Equation 3.3) and therefore permits computation of the angle at which diffraction may occur from a particular set of planes in a crystal.

3.2.4 The Intensity of Diffraction Peaks

The intensities of diffraction lines depend on the atomic locations, site occupancies and thermal motion *[26]*. It can be shown *[26]* that the integrated intensity diffracted from phase A, as measured by a diffractometer with fixed receiving slit and neglecting air absorption, can be expressed as

$$I_{(hkl)A} = \frac{K_e K_{(hkl)A} v_A}{\mu_s}, \tag{3.9}$$

where K_e is a constant for a particular experimental system and depends on the incident-beam intensity, distance from the specimen to the detector and wavelength of the X-radiation;

$K_{(hkl)A}$ is a constant for each diffraction reflection hkl from the crystal structure of phase A and depends on the multiplicity for reflection hkl of phase A, the volume of the unit cell of phase A, diffraction angle, anomalous scattering and temperature effects;

μ_s is the linear attenuation coefficient of the sample;

v_A is the volume fraction of phase A in the sample.

3.2.5 Instrumentation

The instrumentation required for X-ray powder diffractometry consists of three basic parts:

1) a source of radiation, consisting of an X-ray tube and a high voltage generator;
2) the detector and counting equipment;
3) the diffractometer.

Various geometric arrangements of the components have been developed over the years of which the parafocusing geometries of the Bragg-Brentano and the Seeman-Bohlin systems are the most popular *[26]*. The Bragg-Brentano arrangement was employed in this study. The Bragg-Brentano arrangement offers a reasonable compromise between mechanical simplicity and performance *[26]*. In a Bragg-Brentano diffractometer, there are five possible movements *[26]*:

1) angular motion of the X-ray tube;
2) angular motion of the specimen;
3) angular motion of the receiving slit;
4) linear motion of the tube to specimen dimension;
5) linear motion of the receiving slit to specimen dimension.

The two-dimensional geometric arrangement of a Bragg-Brentano diffractometer is depicted in Figure 3.2.

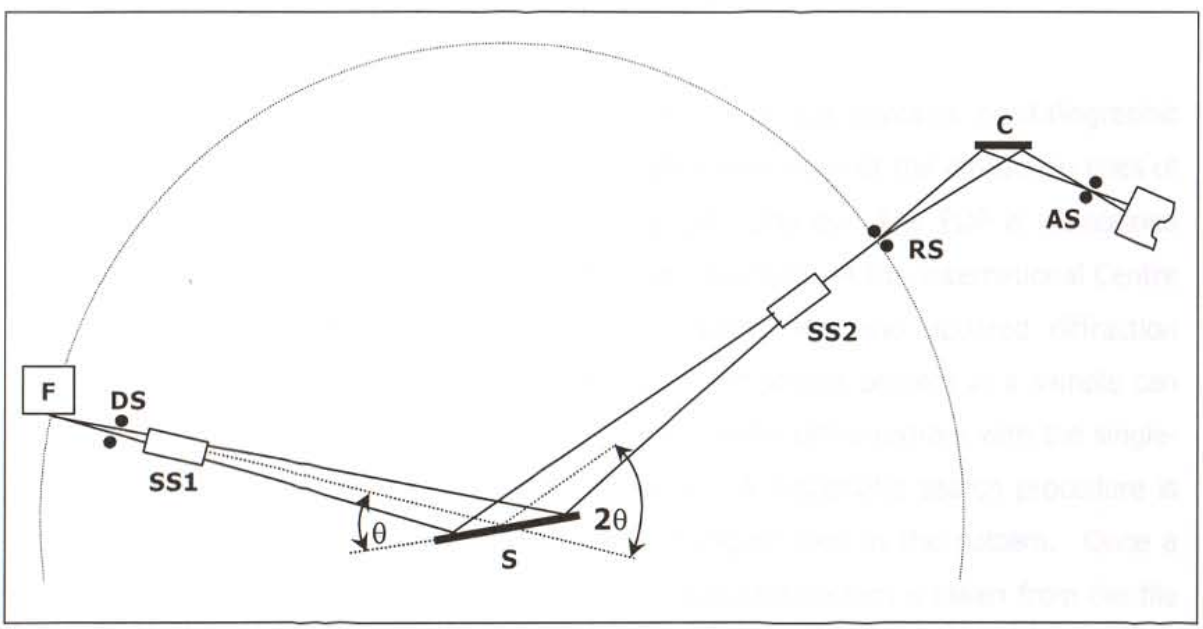

Figure 3.2: Geometric arrangement of the Bragg-Brentano diffractometer

In Figure 3.2, a divergent beam of radiation coming from the line of focus (F) of the X-ray tube passes first through a divergence slit (DS), then through a parallel plate set collimator (Soller slits) (SS1), before striking the specimen (S) at an angle θ. The diffracted rays then leave the specimen at an angle 2θ to the incident beam (and θ to the specimen surface), pass through a second parallel plate collimator (SS2), through the receiving slit (RS), to the detector. A diffracted beam-monochromator, consisting of a crystal (C) and a detector slit (AS), may be placed between the receiving slit and the detector. In order to establish the parafocusing condition, the axes of the line focus of the X-ray tube and the receiving slit are at

equal distances from the axis of the specimen. The X-rays are collected by a suitable radiation detector. In this study, a position sensitive detector was used.

3.2.6 Qualitative Phase Analysis

As already discussed, a powder diffraction measurement of a crystalline material will yield the complete set of Bragg angles in the measurement range, which can be regarded as a fingerprint of the investigated crystallographic phase. In a powder sample containing several crystallographic phases, the fingerprint of each phase is superimposed to yield the powder diffractogram.

The Powder Diffraction File (PDF) is a database that contains crystallographic information such as d-spacings and the relative intensities of the diffraction lines of (currently) approximately 70 000 crystallographic phases. The PDF is maintained by the Joint Committee on Powder Diffraction Standards at the International Centre for Diffraction Data, USA, by continually adding new and updated diffraction patterns to the file *[26, 27]*. The crystallographic phases present in a sample can be qualitatively determined by comparing the powder diffractogram with the single-phase reference patterns in the PDF database. A systematic search procedure is generally used and is based on the three strongest lines in the pattern. Once a potential match is indicated, the appropriate standard pattern is taken from the file and all lines are subtracted. This procedure is repeated until all significant lines in the unknown pattern are accounted for.

3.3 X-ray Diffraction Analysis of Prepared Samples

X-ray diffractograms of all samples were obtained on a Siemens D5000 X-ray diffractometer with Bragg-Brentano geometry. The following instrument variables were found suitable for recording of the diffractograms: Generator: 50 mA, 40 kV; X-ray tube: CuK_α (λ = 1.5406 Å); Angular Range: 15-75 °2θ; Detector: Position sensitive detector; Step size/count time: 0.0156 °2θ/4 s.

The selected power settings for the generator provided sufficient intensities for the diffractograms. The wavelength of the CuK_α-radiation provided a reasonable

dispersion of the pattern and at the same time a reasonable d-spacing range (or angular range) that could be scanned *[26]*. The chosen angular range contained a sufficient number of lines for each phase to allow for qualitative analysis. In addition, most of the diffraction patterns considered from the PDF database fitted into the chosen angular range.

The position sensitive detector allowed recording of data from a range of angles at one time, which drastically reduced recording times for a given step size/count time setting. The selected step size was typical for fairly well crystallized materials *[26]* and produced well-defined peaks in the diffractograms. The selected count time of 4 seconds per step was considered sufficient as increasing the count time beyond this time did not significantly improve the peak definition in the diffractograms. A count time of 4 s per selected step size corresponded to a total recording time of approximately 60 minutes per sample. The effects of changing the count time can be seen in Figure 3.3.

3.3.1 X-ray Diffraction Patterns of Phases Detected in Prepared Samples

Diffrac^{Plus} software was used for the evaluation of the diffractograms together with the crystallographic data from the 1995 Powder Diffraction File-2 (Set 45), release A6, published by the International Centre for Diffraction Data. In Table 3.2, the crystallographic data of the detected phases are summarised. The symbols a, b and c in Table 3.2 signify the edges of the unit cell, while α, β and γ denote the angles between c/b, c/a and a/b, respectively. The numbers in brackets indicate the PDF data set numbers. The complete data sets for these phases, as obtained from the PDF, are given in Appendix A.

The relative positions and the relative intensities of the ten most intense reflections of each phase that was detected in one or more of the prepared samples or raw materials, are shown in Figures 3.4 to 3.18.

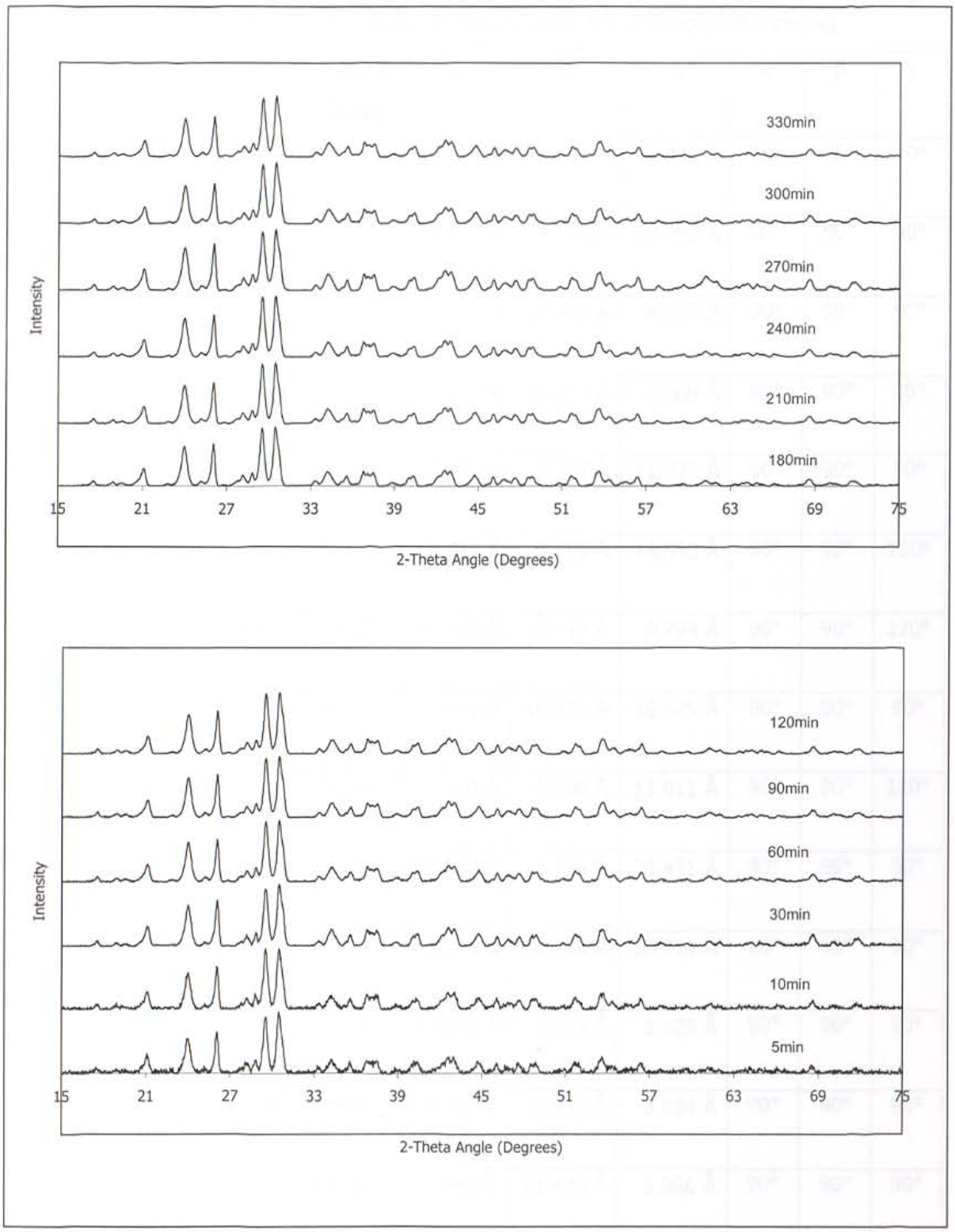

Figure 3.3: Effect of total scan time on resolution of peaks in a diffractogram

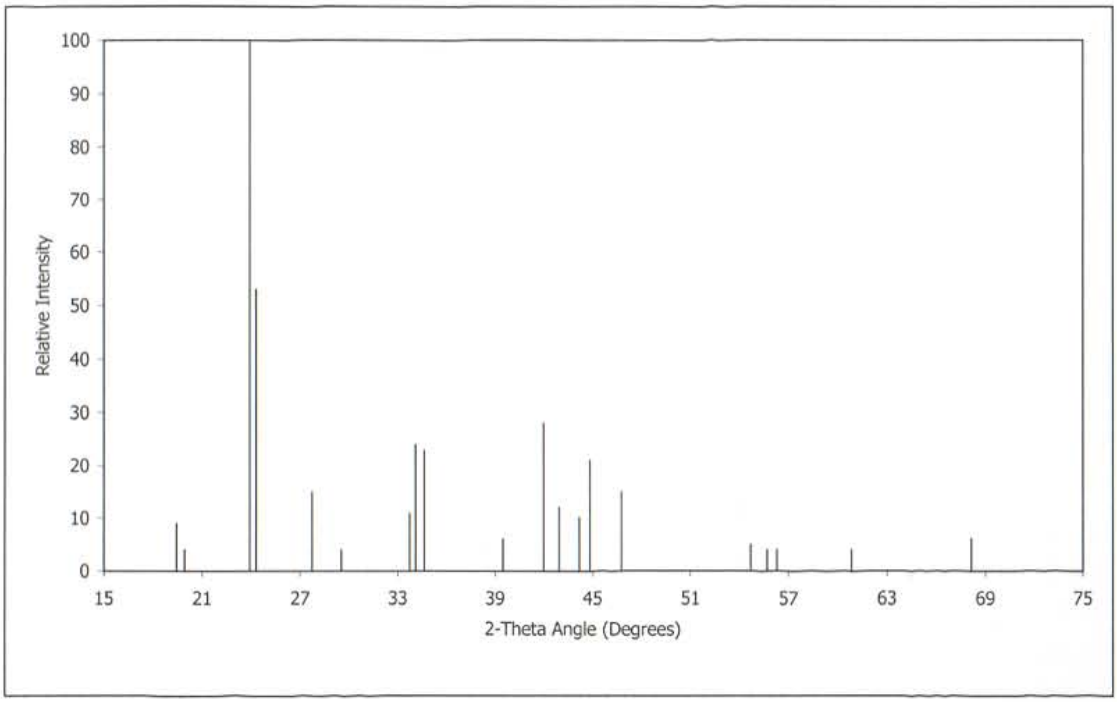

Figure 3.4: Reference pattern of $BaCO_3$ showing the ten most intense reflections (PDF number: 5-378)

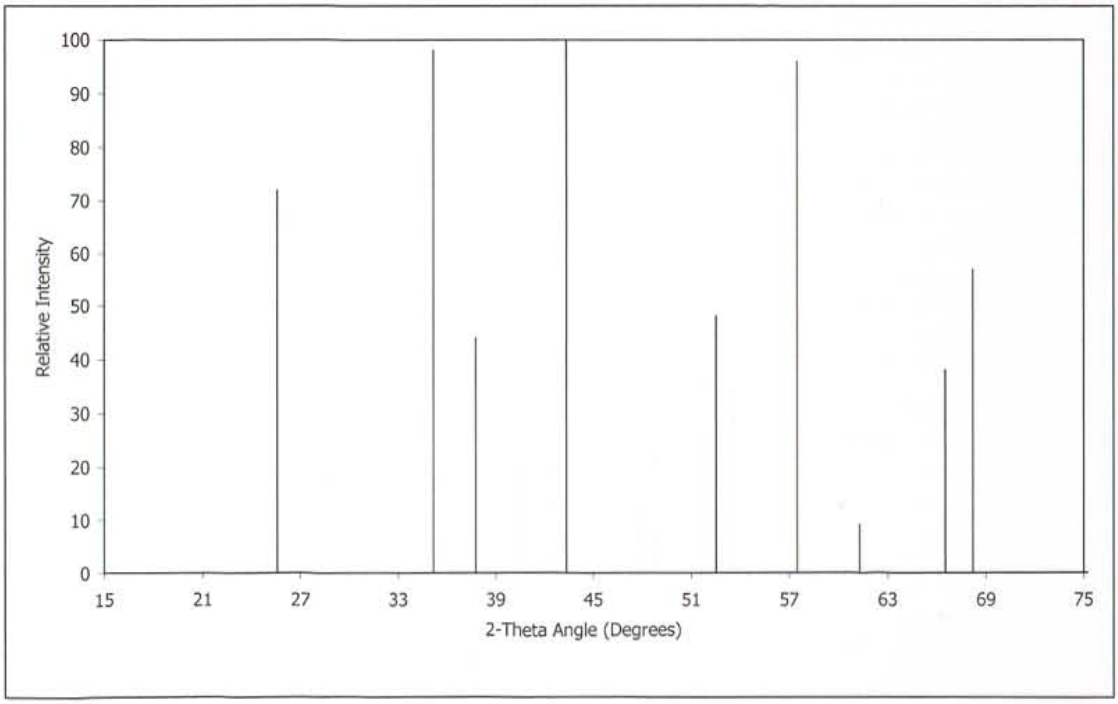

Figure 3.5: Reference pattern of Al_2O_3 showing the ten most intense reflections (PDF number: 43-1484)

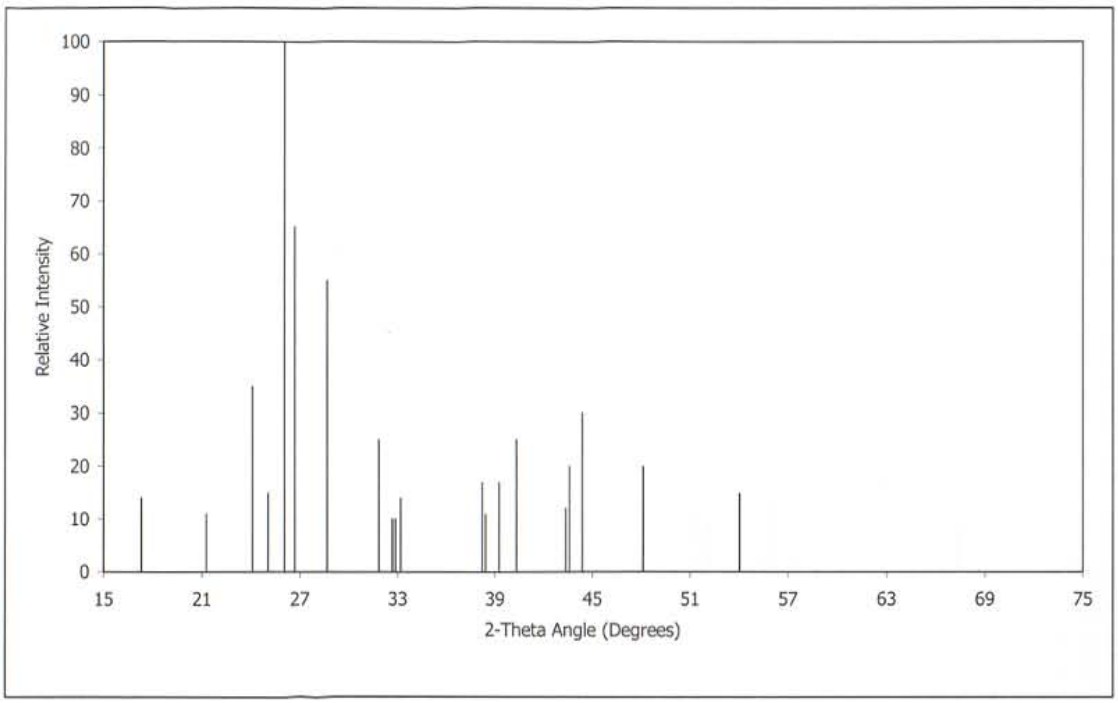

Figure 3.6: Reference pattern of $BaO.SiO_2$ showing the ten most intense reflections (PDF number: 26-1402)

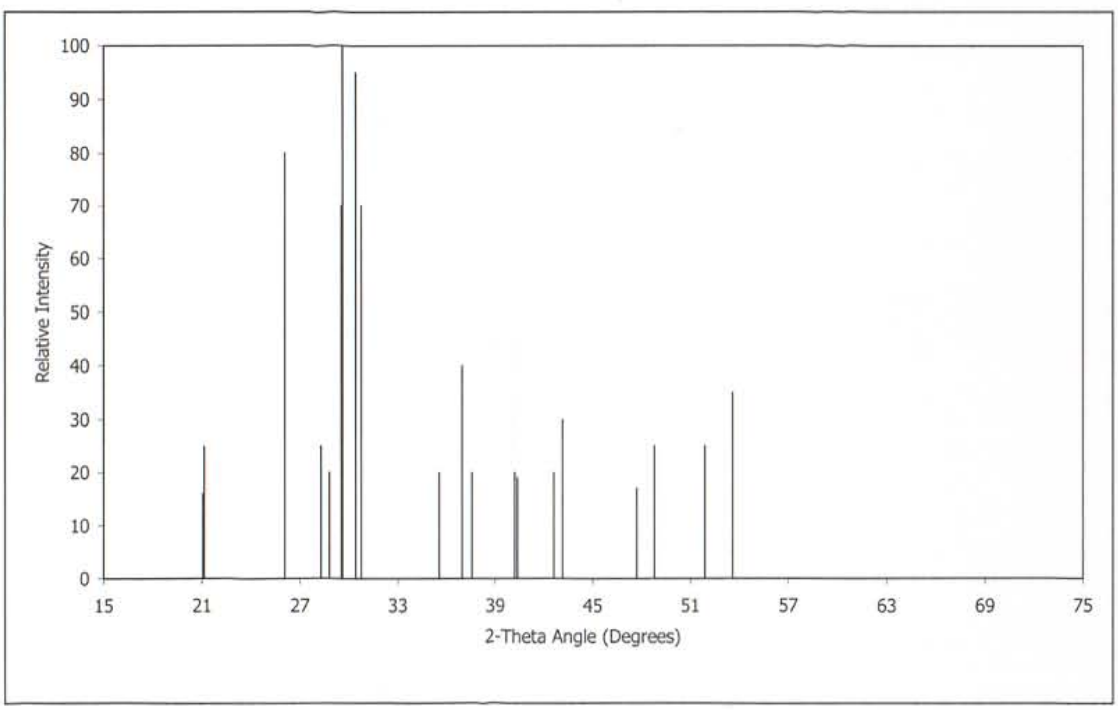

Figure 3.7: Reference pattern of $2BaO.SiO_2$ showing the ten most intense reflections (PDF number: 26-1403)

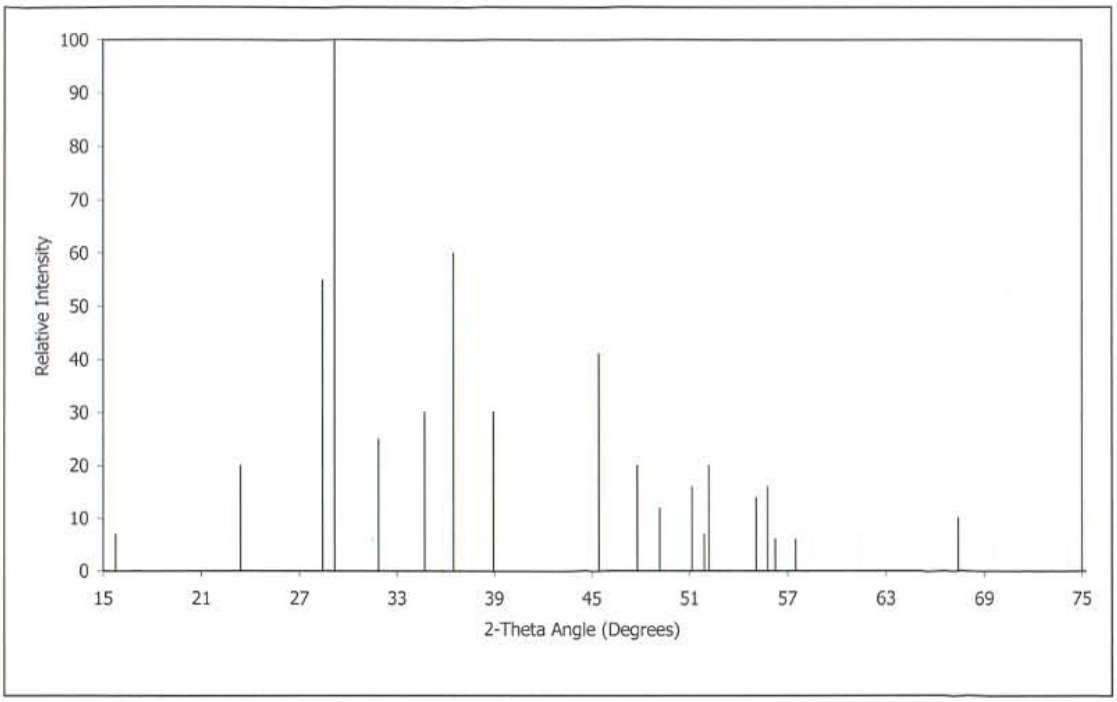

Figure 3.8: Reference pattern of $3BaO.SiO_2$ showing the ten most intense reflections (PDF number: 26-180)

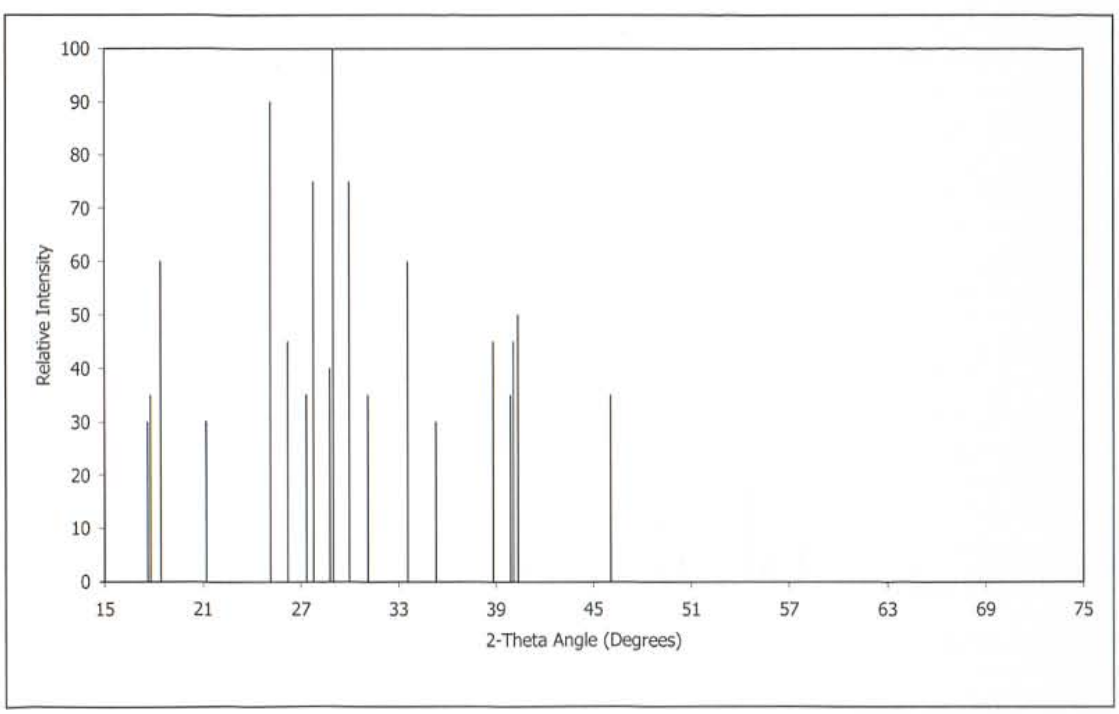

Figure 3.9: Reference pattern of $BaO.Al_2O_3.SiO_2$ showing the ten most intense reflections (PDF number: 21-806)

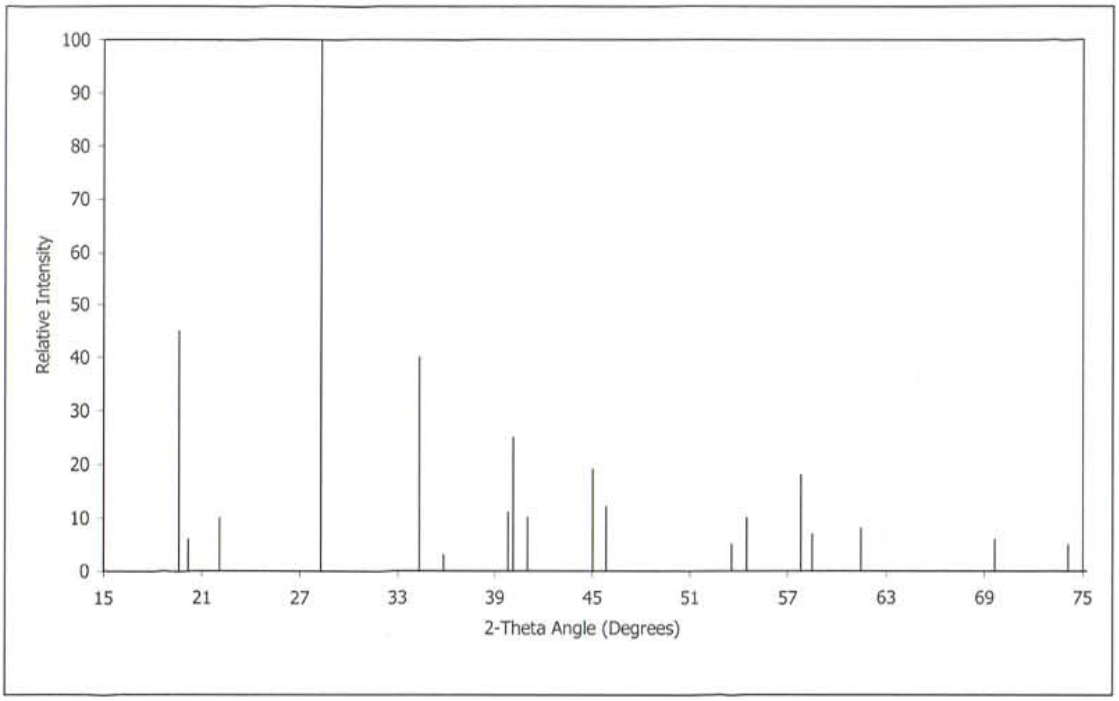

Figure 3.10: Reference pattern of $BaO.Al_2O_3$ showing the ten most intense reflections (PDF number: 17-306)

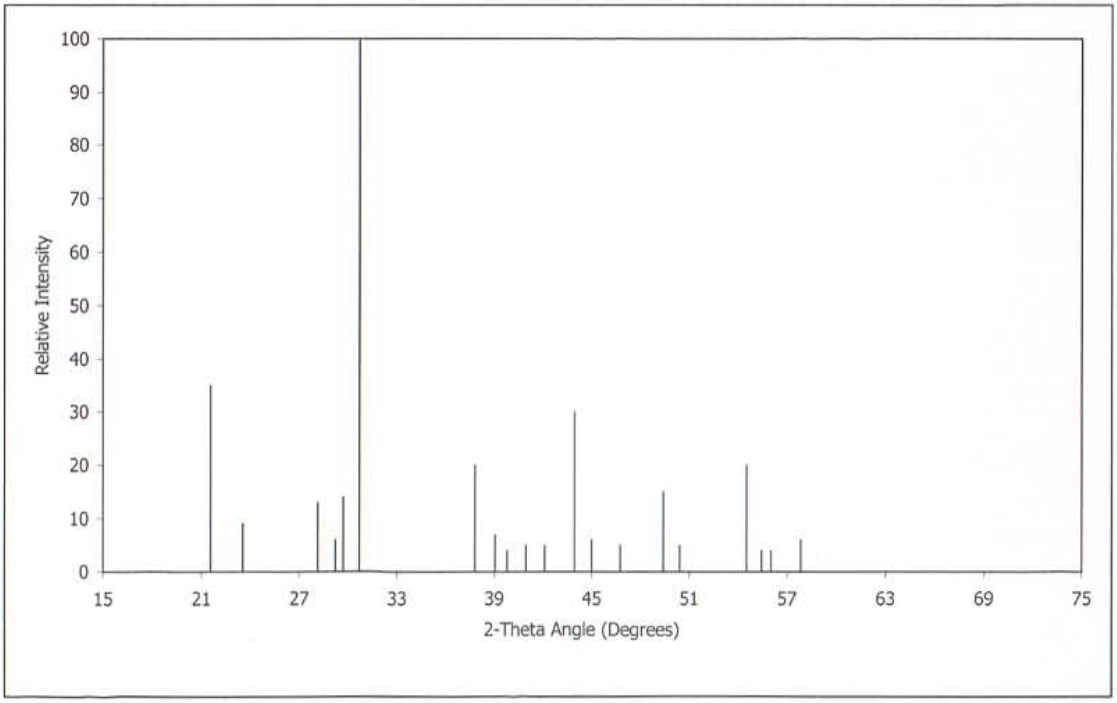

Figure 3.11: Reference pattern of $3BaO.Al_2O_3$ showing the ten most intense reflections (PDF number: 25-75)

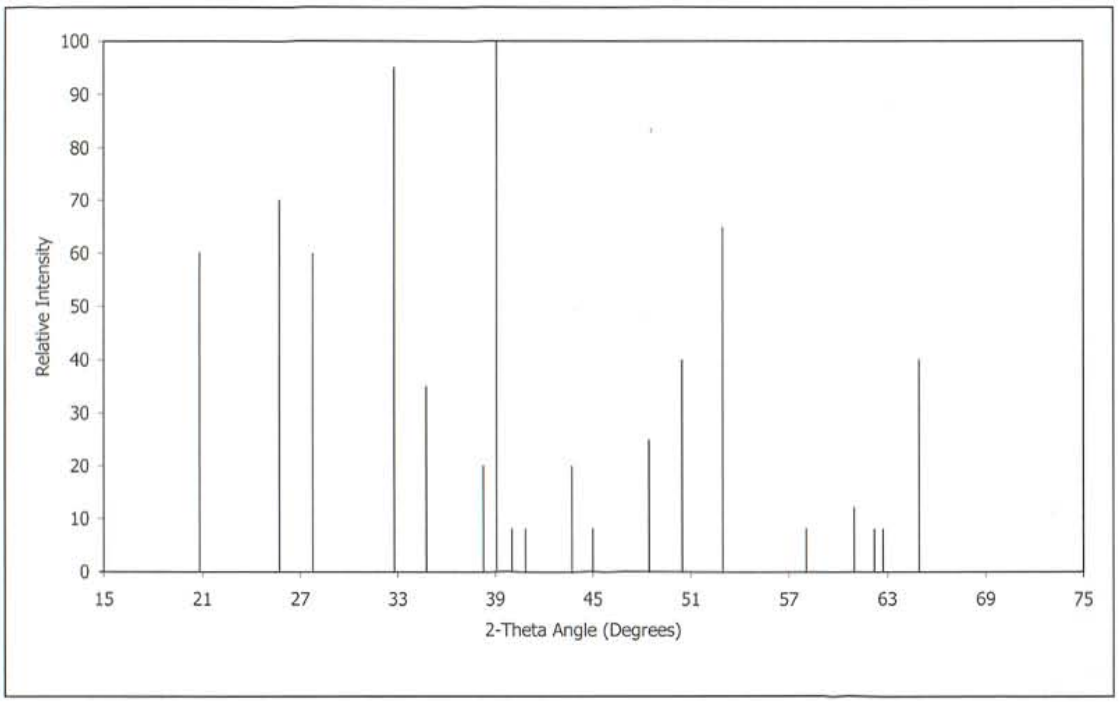

Figure 3.12: Reference pattern of $BaO.2Fe_2O_3$ showing the ten most intense reflections (PDF number: 25-1476)

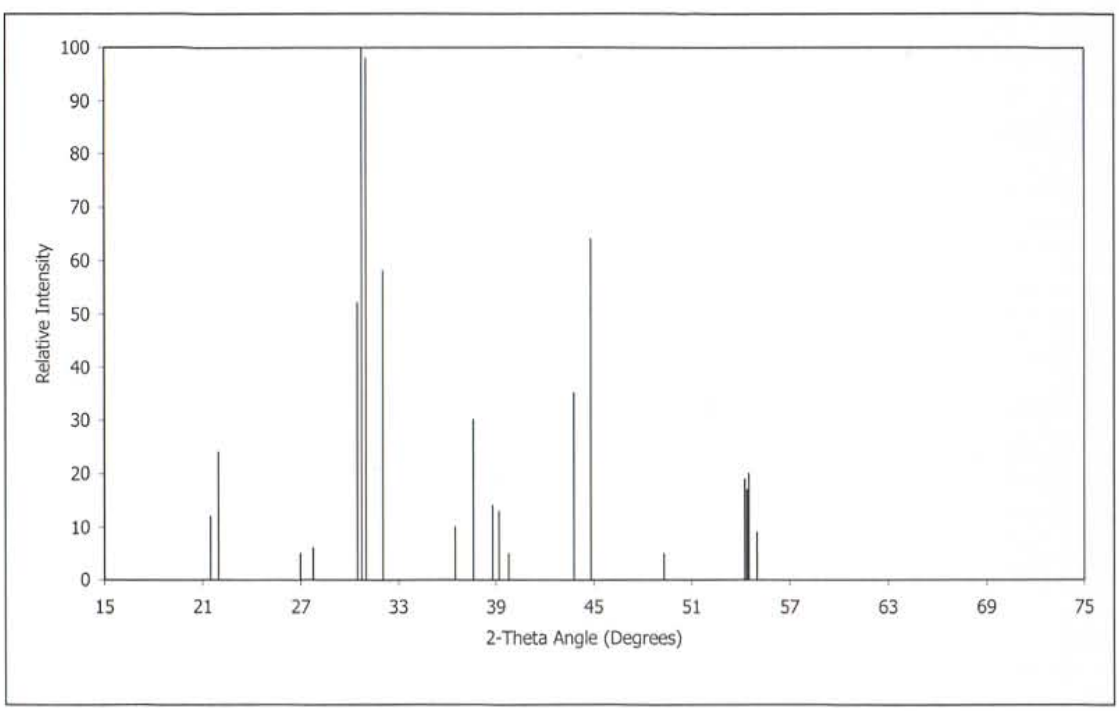

Figure 3.13: Reference pattern of $2BaO.Fe_2O_3$ showing the ten most intense reflections (PDF number: 43-256)

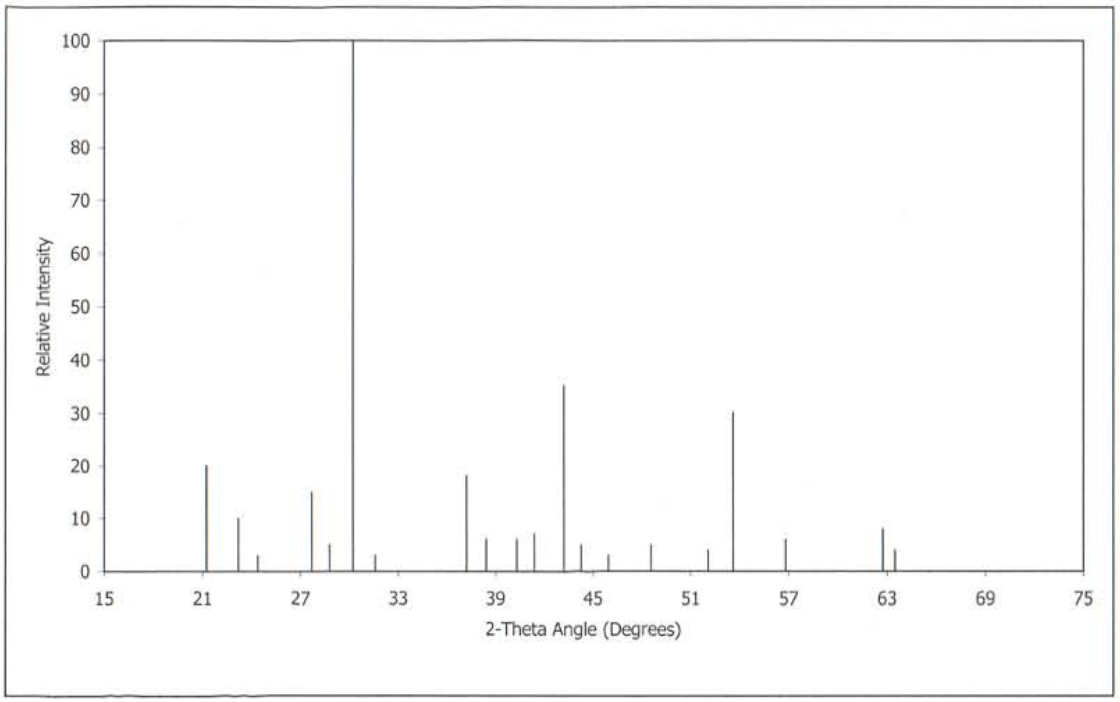

Figure 3.14: Reference pattern of $3BaO.Fe_2O_3$ showing the ten most intense reflections (PDF number: 25-1477)

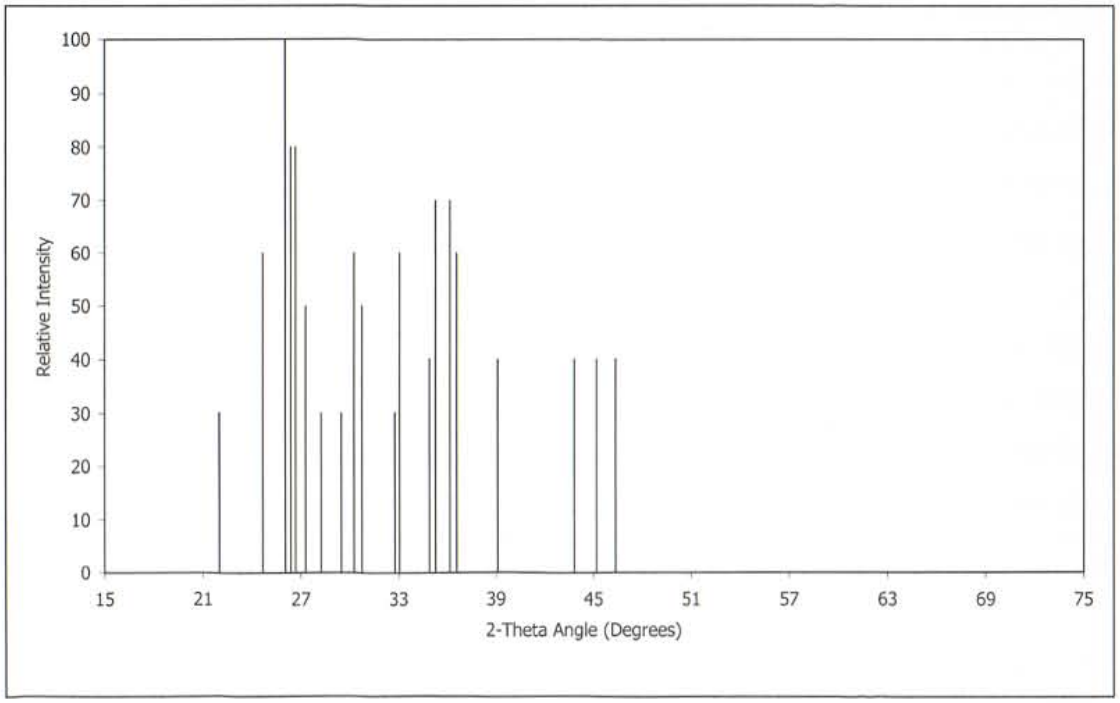

Figure 3.15: Reference pattern of $Ba(OH)_2$ showing the ten most intense reflections (PDF number: 44-585)

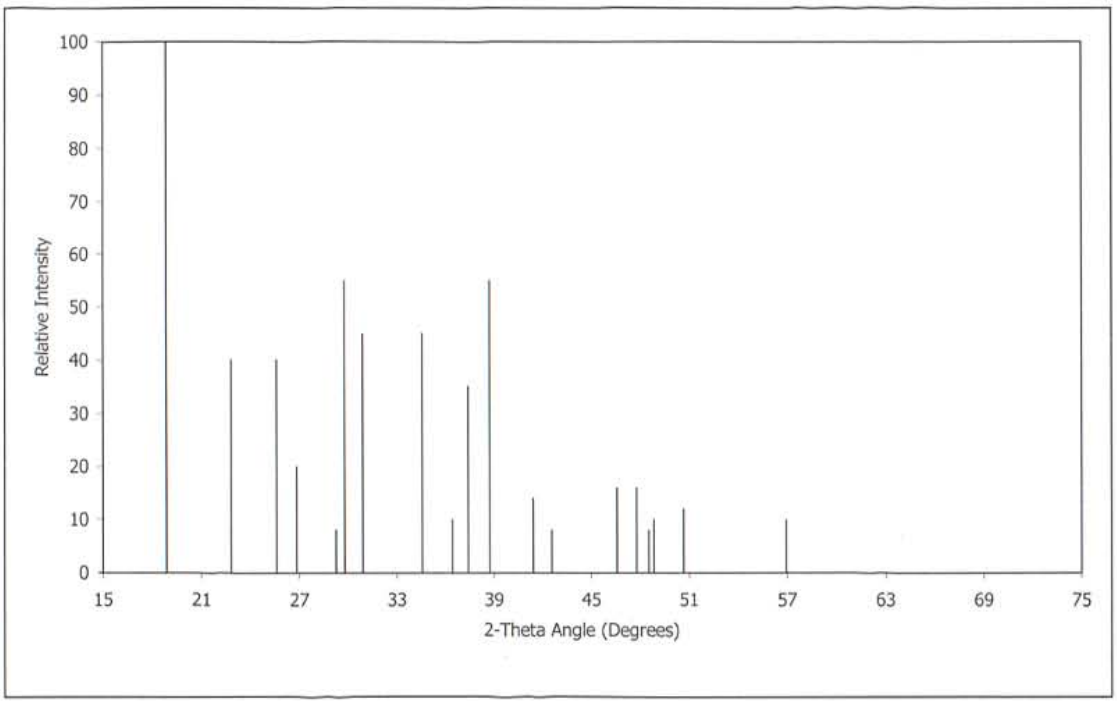

Figure 3.16: Reference pattern of $Ba(OH)_2.H_2O$ showing the ten most intense reflections (PDF number: 26-154)

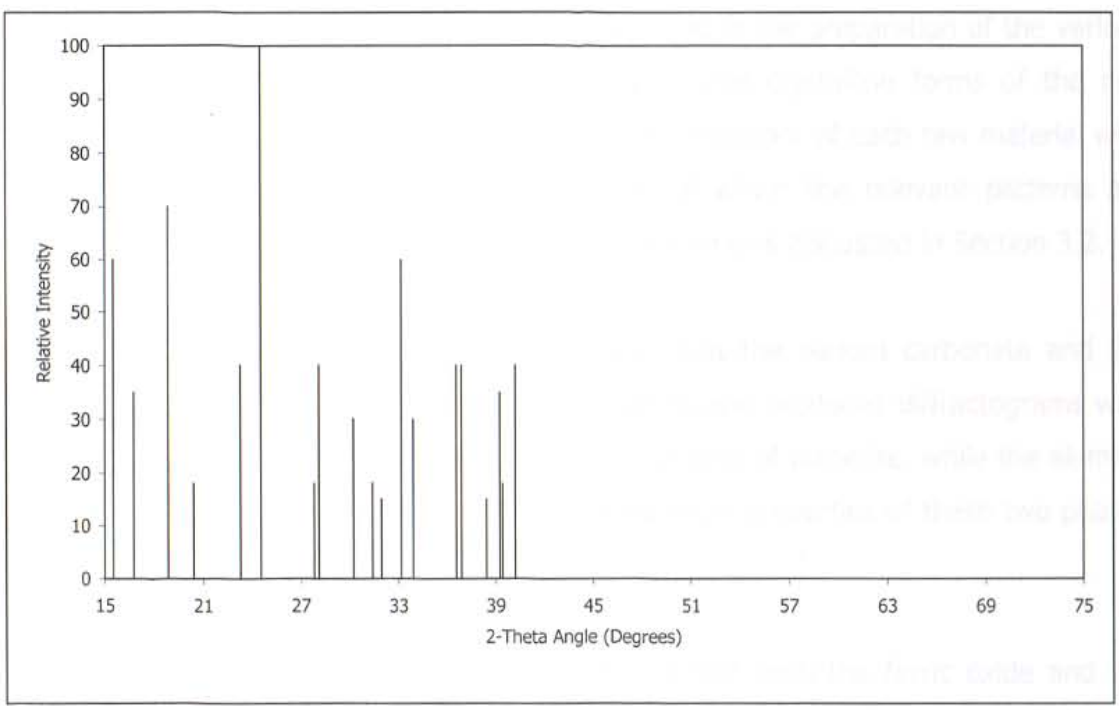

Figure 3.17: Reference pattern of $Ba(OH)_2.3H_2O$ showing the ten most intense reflections (PDF number: 33-153)

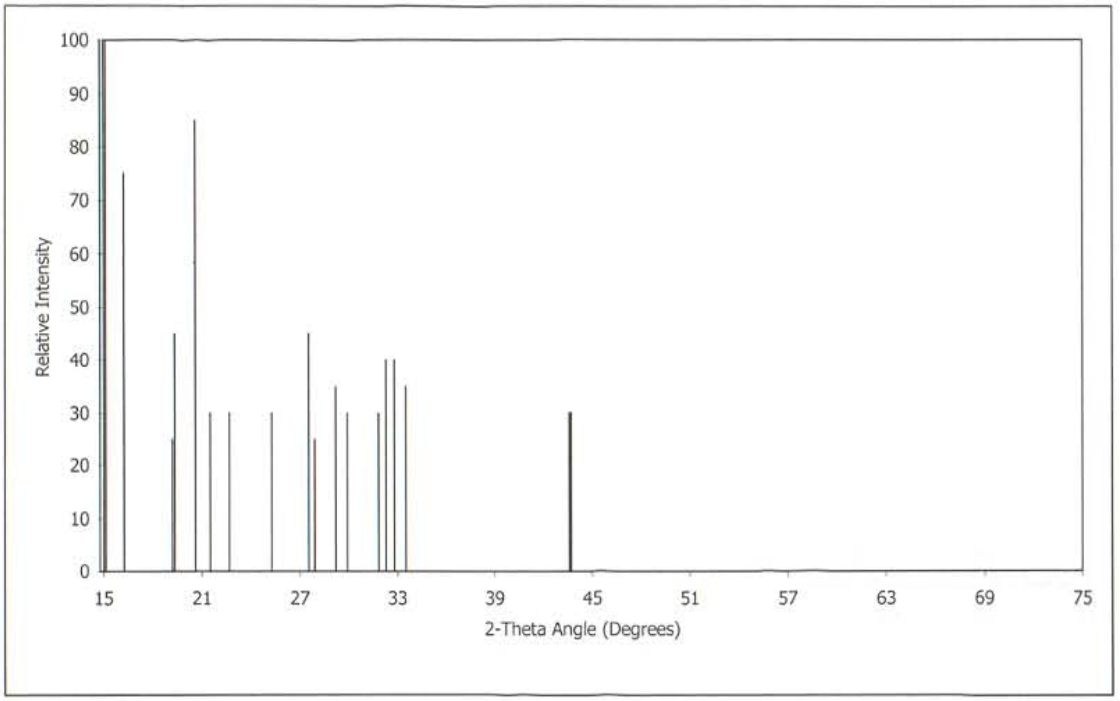

Figure 3.18: Reference pattern of $Ba(OH)_2.8H_2O$ showing the ten most intense reflections (PDF number: 26-155)

3.4 Crystalline Phases of the Raw Materials

The diffractograms of the four raw materials used in the preparation of the various samples are shown in Figures 3.19 to 3.22. The crystalline forms of the raw materials were identified by comparing the diffractogram of each raw material with the reference patterns in the PDF database of which the relevant patterns are shown in Section 3.3. This identification technique was discussed in Section 3.2.

From Figures 3.19 and 3.20, it can be seen that the barium carbonate and the aluminium oxide both appeared to be crystalline and produced diffractograms with sharp peaks. The barium carbonate was in the form of witherite, while the alumina was in the form of corundum. The crystallographic properties of these two phases are given in Table 3.2.

Considering Figures 3.21 and 3.22, it appears that both the ferric oxide and the precipitated silica were amorphous and therefore did not produce any well-defined peaks in their diffractograms.

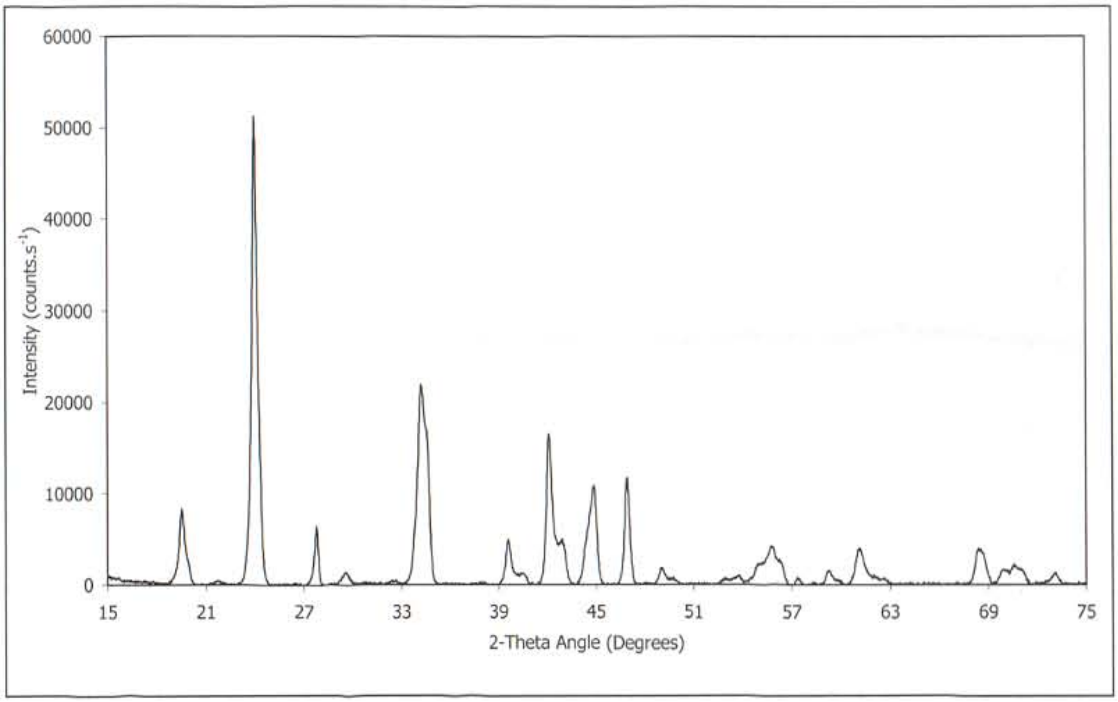

Figure 3.19: Diffractogram of barium carbonate (witherite)

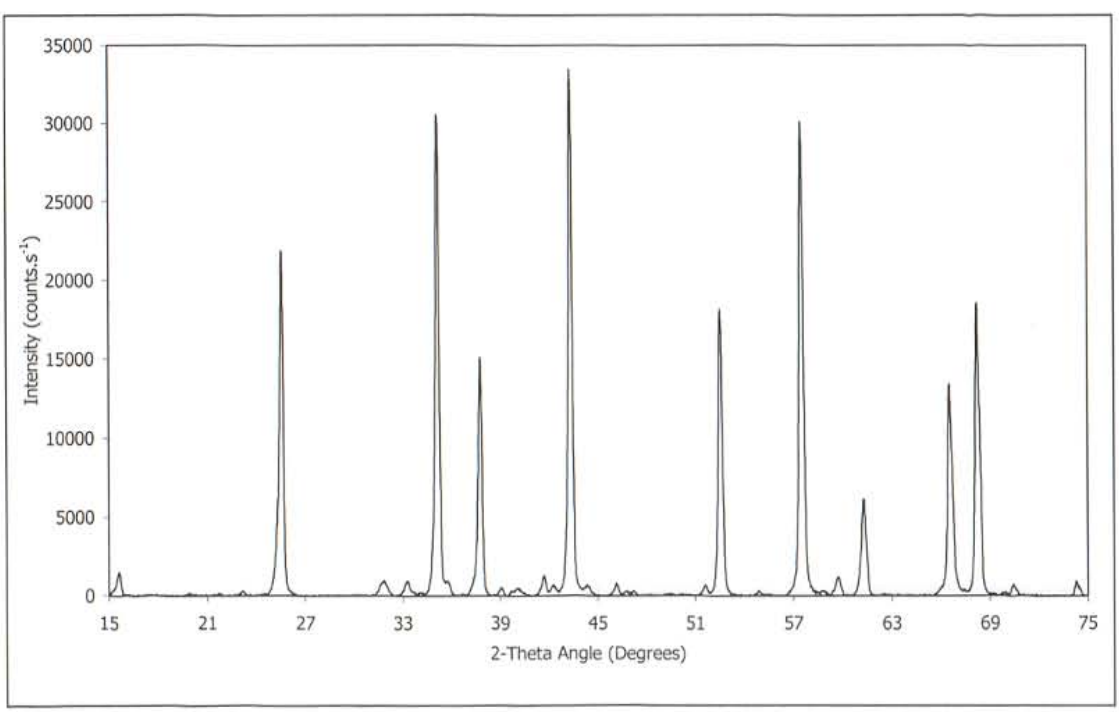

Figure 3.20: Diffractogram of aluminium oxide (corundum)

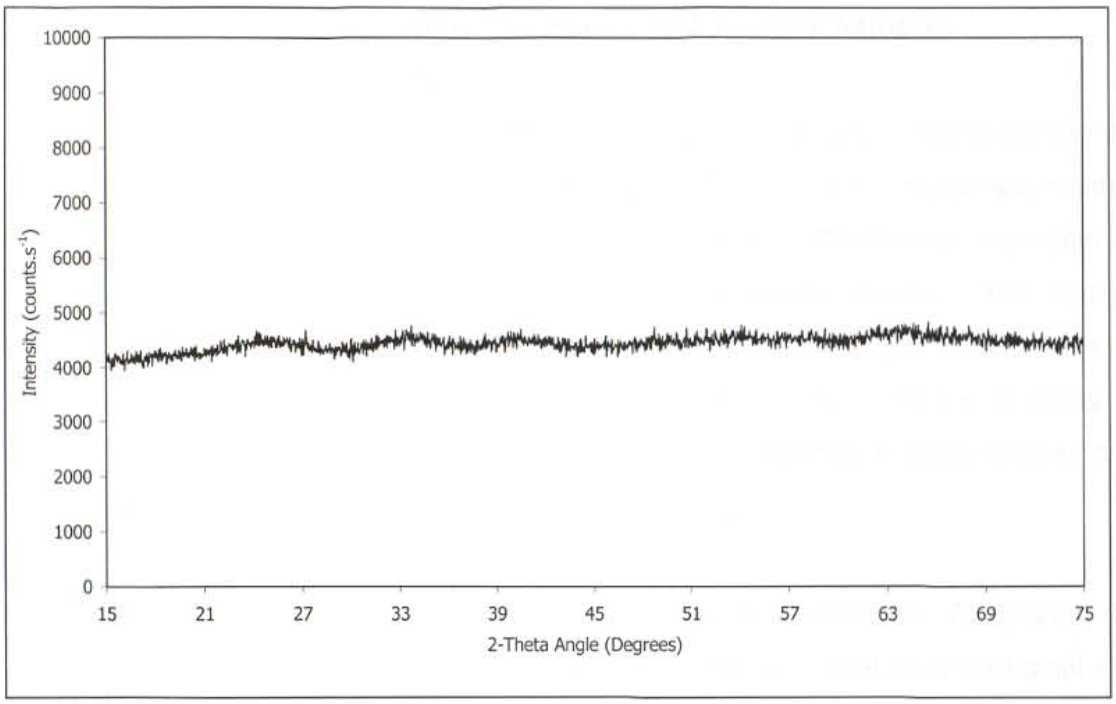

Figure 3.21: Diffractogram of ferric oxide (amorphous)

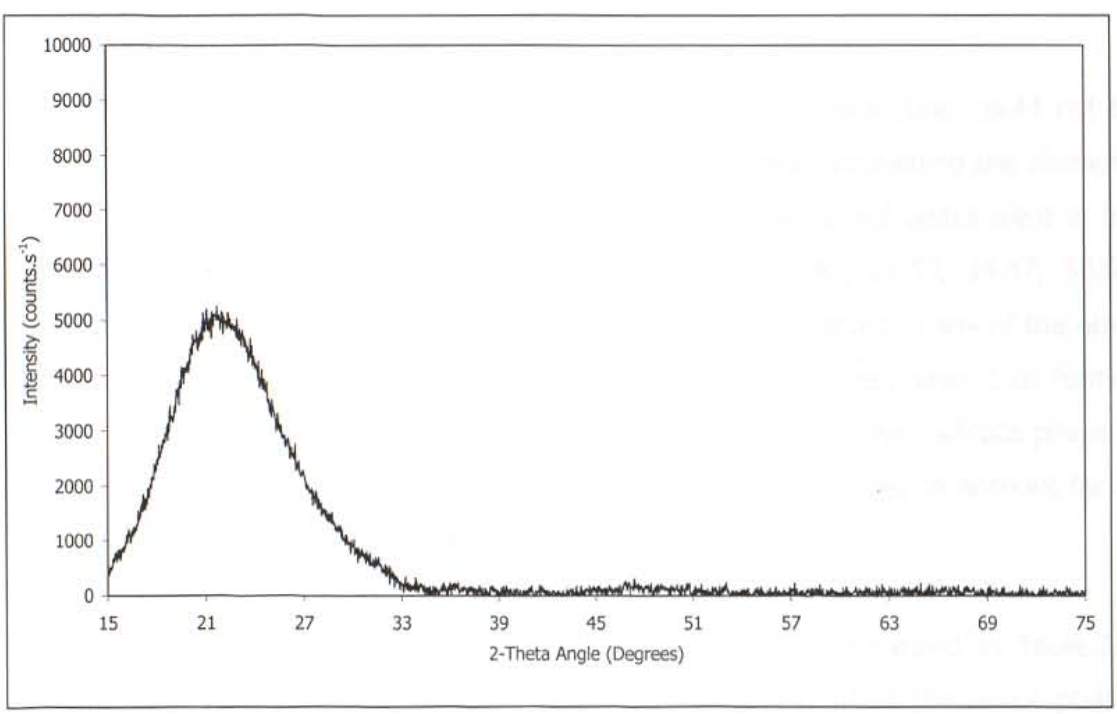

Figure 3.22: Diffractogram of precipitated silicon dioxide (amorphous)

3.5 Crystalline Phases Formed in the Binary and Ternary Samples

3.5.1 The Binary System BaO-SiO_2

The diffractograms of the samples prepared from the binary mixtures containing barium carbonate and silica are shown in Figures 3.23 to 3.25. The sample mixture with the molar ratio of $BaCO_3$:SiO_2 = 1:1, yielded mainly orthorhombic monobarium silicate and a small quantity of orthorhombic dibarium silicate. The sample mixtures with molar ratios of $BaCO_3$:SiO_2 = 2:1 and 3:1, both produced a mixture of phases consisting of orthorhombic dibarium silicate and a smaller quantity of tetragonal tribarium silicate. This mixture of phases persisted in these two samples even after heating for 480 or 550 hours.

No uncombined BaO was detected in any of these three samples. Comparing the molar ratios of BaO:SiO_2 in the phases that formed with that in the original raw mixtures, it appears that some uncombined silica should still be present in the samples with molar ratios = 1:1 and 2:1, in order to account for all the silica. However, due to the amorphicity of the silica used, the presence of uncombined silica could not be confirmed by X-ray diffraction.

The sample with a molar ratio of 3:1 had a number of peaks that could not be resolved using the reference patterns in the PDF of phases containing the elements Ba, O, Si, C and H (or combinations thereof). The unidentified peaks were at the following 2θ angles (degrees): 26.51, 26.91, 27.17, 31.48, 32.53, 34.47, 38.61, 39.67, 40.61, 41.99 and 43.47. These peaks were not observed in any of the other samples prepared during this study. If the molar ratios in the phases that formed are compared with that in the raw mixture, it appears that barium silicate phase(s) with molar ratio(s) of BaO:SiO_2 > 3:1 must have formed in order to account for all the $BaCO_3$ in the raw mixture.

The crystalline phases identified in these samples are summarized in Table 3.3. The major phases produced peaks with high intensities, while the minor phases produced only small peaks with low intensities. (See Table 3.2 or Appendix A for a more complete description of the phases.)

Table 3.3: Crystalline phases identified in samples prepared from mixtures containing $BaCO_3$ and SiO_2 in various molar ratios

Molar Ratio $BaCO_3$:SiO_2	Temperature (°C)	Heating Time (hours)	Major Phase(s)	Minor Phase(s)
1:1	1400	120	$BaO.SiO_2$	$2BaO.SiO_2$
2:1	1400	480	$2BaO.SiO_2$ $3BaO.SiO_2$	none detected
3:1	1400	550	$2BaO.SiO_2$ $3BaO.SiO_2$	unidentified peaks

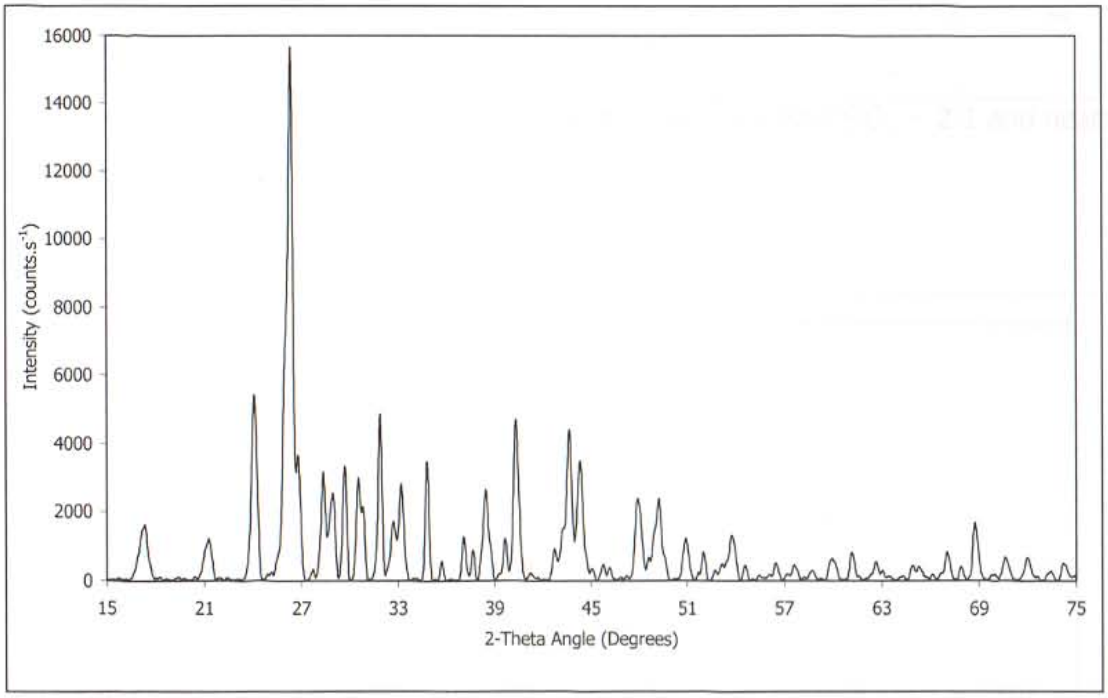

Figure 3.23: Diffractogram of sample with molar ratio $BaO:SiO_2$ = 1:1 and heated at 1400 °C for 120 hours

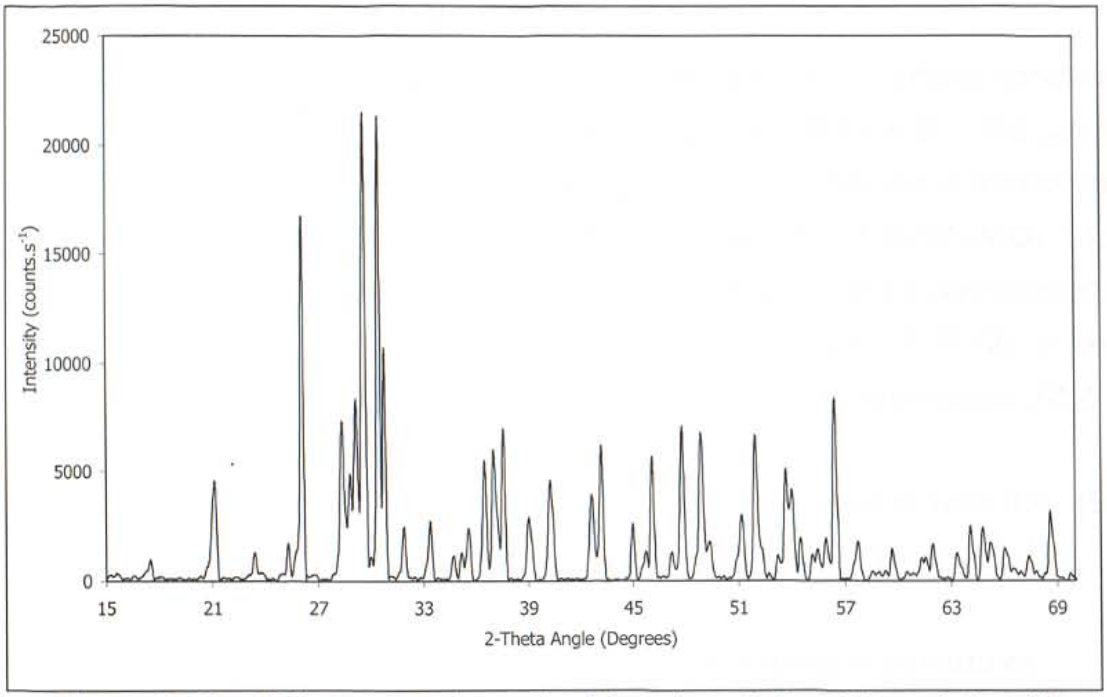

Figure 3.24: Diffractogram of sample with molar ratio $BaO:SiO_2$ = 2:1 and heated at 1400 °C for 480 hours

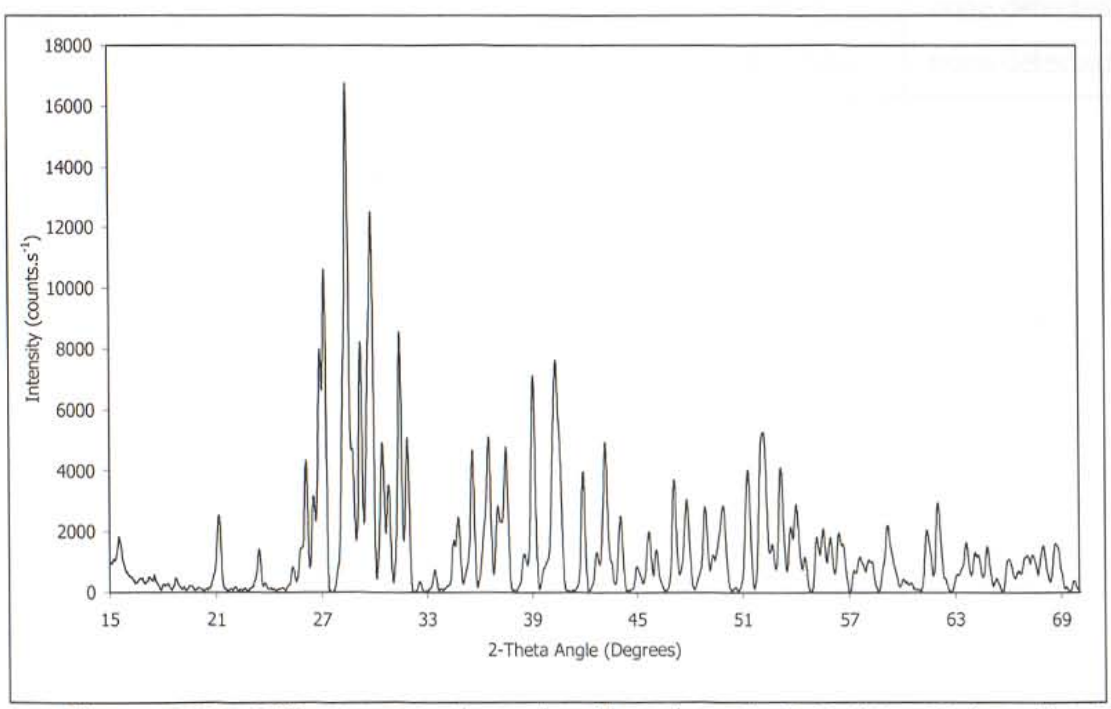

Figure 3.25: Diffractogram of sample with molar ratio $BaO:SiO_2$ = 3:1 and heated at 1400 °C for 550 hours

3.5.2 The Binary System BaO-Al_2O_3

The diffractograms of the samples prepared from the binary mixtures containing barium carbonate and alumina are shown in Figures 3.26 to 3.27. The sample mixture with the molar ratio of $BaCO_3$:Al_2O_3 = 1:1, yielded hexagonal monobarium aluminate, while the sample mixture with the molar ratio of $BaCO_3$:Al_2O_3 = 3:1, produced cubic tribarium aluminate. No uncombined BaO or Al_2O_3 was detected in the two samples. The relatively broad band in the region of 15 °2θ in both diffractograms indicates the possible presence of some amorphous material *[26]*.

The crystalline phases identified in these two samples are listed in Table 3.4. (See Table 3.2 or Appendix A for a more complete description of the phases.)

Table 3.4: Crystalline phases identified in samples prepared from mixtures containing $BaCO_3$ and Al_2O_3 in various molar ratios

Molar Ratio $BaCO_3$:Al_2O_3	Temperature (°C)	Heating Time (hours)	Major Phase(s)	Minor Phase(s)
1:1	1200	18	$BaO.Al_2O_3$	none detected
3:1	1400	40	$3BaO.Al_2O_3$	none detected

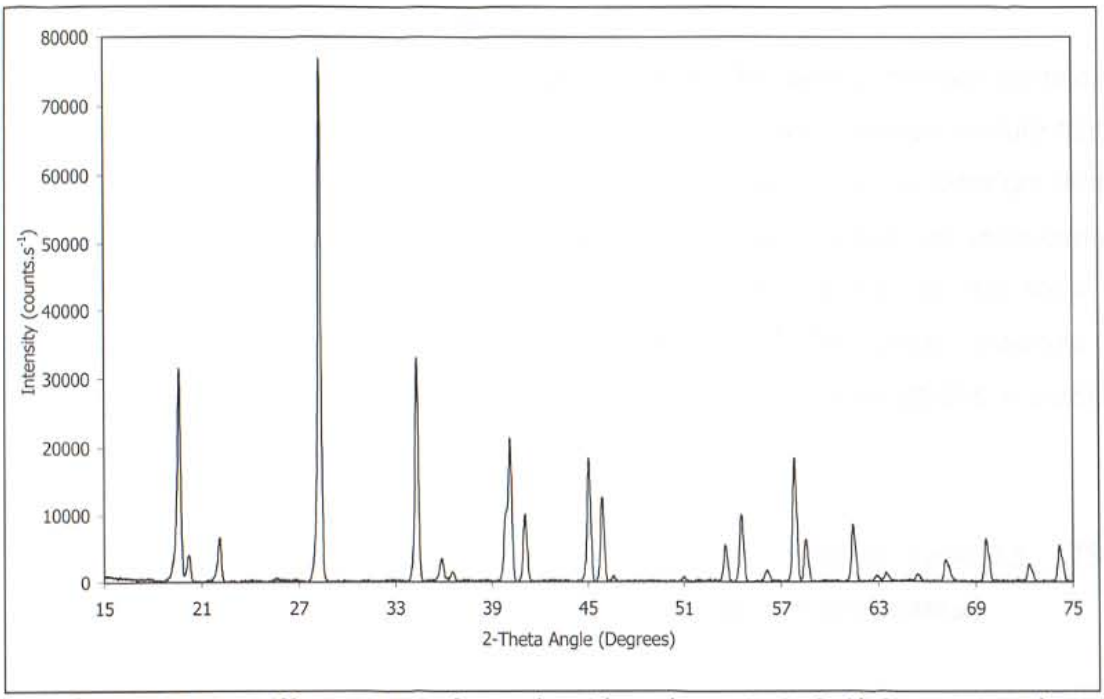

Figure 3.26: Diffractogram of sample with molar ratio $BaO:Al_2O_3$ = 1:1 and heated at 1200 °C for 18 hours

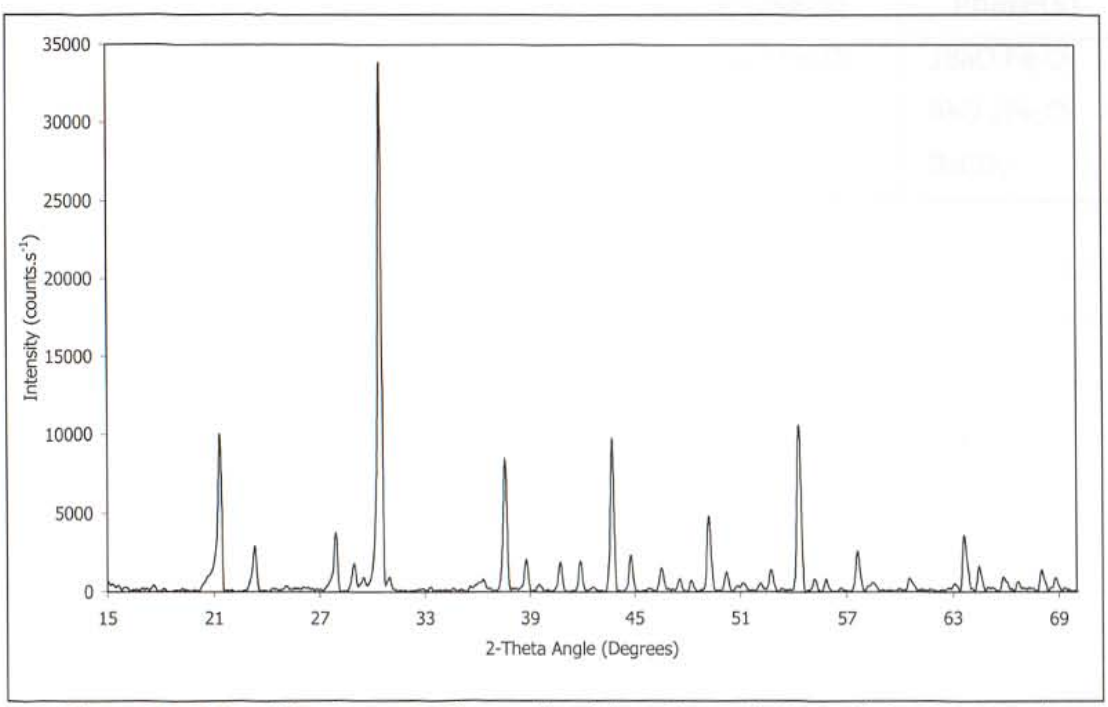

Figure 3.27: Diffractogram of sample with molar ratio $BaO:Al_2O_3$ = 3:1 and heated at 1400 °C for 40 hours

3.5.3 The Binary System BaO-Fe_2O_3

The diffractogram of the sample prepared from the binary mixture containing barium carbonate and ferric oxide is shown in Figure 3.28. The raw mixture had a molar ratio of $BaCO_3$:Fe_2O_3 = 2:1 and yielded mainly the monoclinic dibarium ferrite phase. Small quantities of cubic tribarium ferrite and hexagonal monobarium diferrite also formed. A small quantity of uncombined BaO in the form of orthorhombic barium carbonate was also detected. The peaks observed in Figure 3.28 are relatively broad. This was probably due to some strains in possibly non-uniform phases *[26]*.

The crystalline phases identified in this sample are listed in Table 3.5. (See Table 3.2 or Appendix A for a more complete description of the phases.)

Table 3.5: Crystalline phases identified in sample prepared from a mixture containing $BaCO_3$ and Fe_2O_3

Molar Ratio $BaCO_3$:Fe_2O_3	Temperature (°C)	Heating Time (hours)	Major Phase(s)	Minor Phase(s)
2:1	1000	16	$2BaO.Fe_2O_3$	$3BaO.Fe_2O_3$ $BaO.2Fe_2O_3$ $BaCO_3$

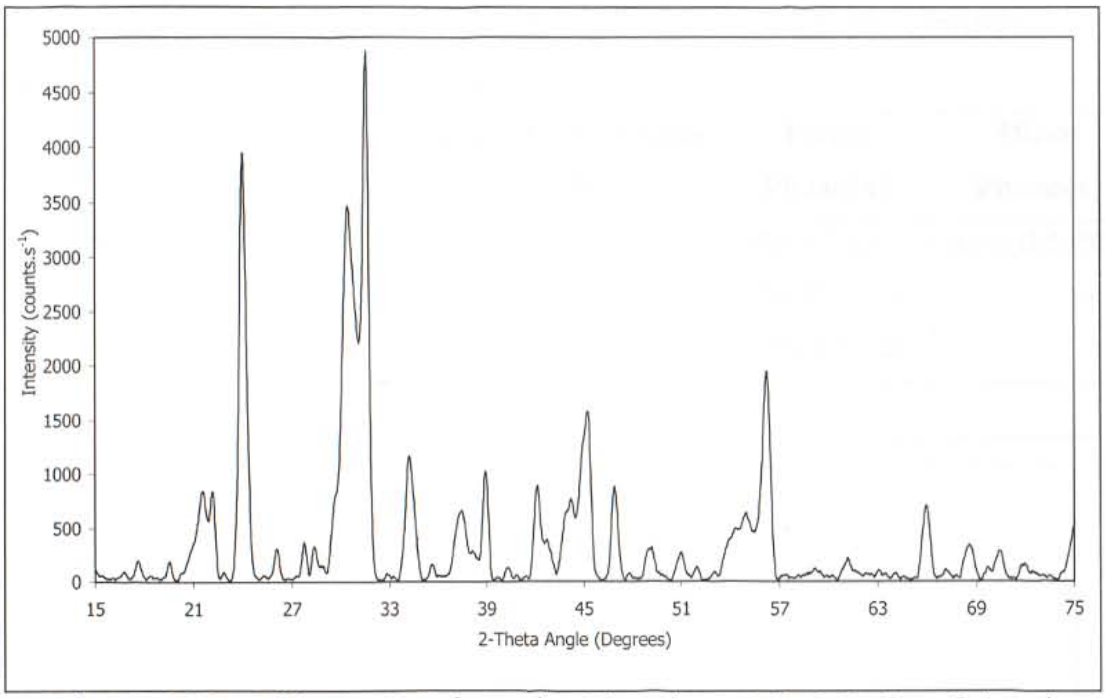

Figure 3.28: Diffractogram of sample with molar ratio $BaO:Fe_2O_3$ = 2:1 and heated at 1000 °C for 16 hours

3.5.4 The Ternary System $BaO\text{-}Al_2O_3\text{-}Fe_2O_3$

The diffractogram of the sample prepared from the ternary mixture containing barium carbonate, alumina and ferric oxide is shown in Figure 3.29. The raw mixture had a molar ratio of $BaCO_3:Al_2O_3:Fe_2O_3$ = 4:1:1 and yielded a mixture of phases consisting of hexagonal monobarium aluminate, monoclinic dibarium ferrite and cubic tribarium ferrite phases. The relatively broad band in the region of 15 °2θ in the diffractogram indicates that some amorphous material is probably also present *[26]*.

The crystalline phases identified in this sample are listed in Table 3.6. (See Table 3.2 or Appendix A for a more complete description of the phases.)

Table 3.6: Crystalline phases identified in sample prepared from a mixture containing $BaCO_3$, Al_2O_3 and Fe_2O_3

Molar Ratio $BaCO_3$:Al_2O_3:Fe_2O_3	Temperature (°C)	Heating Time (hours)	Major Phase(s)	Minor Phase(s)
4:1:1	1100	500	$BaO.Al_2O_3$ $2BaO.Fe_2O_3$ $3BaO.Fe_2O_3$	none detected

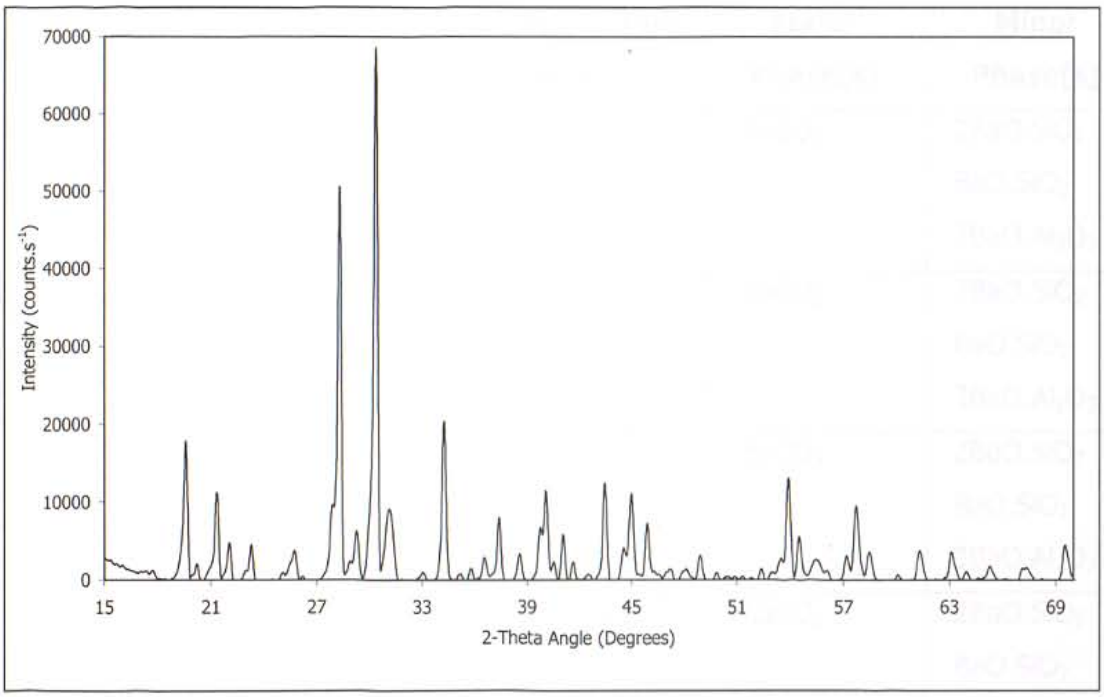

Figure 3.29: Diffractogram of sample with molar ratio $BaO:Al_2O_3:Fe_2O_3$ = 4:1:1 and heated at 1100 °C for 500 hours

3.6 Crystalline Phases Formed in the Quaternary Samples

The diffractograms of the quaternary samples heated at 900 °C for 60 minutes are shown in Figure 3.30. The BSF of the samples varied between 86 % and 102 % in steps of 4 %, while the silica modulus and the alumina modulus were both constant in all mixes at 2.3 and 1.5, respectively. After heating at 900 °C, all samples contained mainly unreacted barium carbonate and a small quantity of orthorhombic dibarium silicate. Some cubic tribarium aluminate and orthorhombic monobarium silicate were also detected. No unreacted alumina was detected in any of the

samples, possibly due to the alumina content being too low to be detected by X-ray diffraction.

The crystalline phases identified in these five samples are listed in Table 3.7. (See Table 3.2 or Appendix A for a more complete description of the phases.)

Table 3.7: Crystalline phases identified in samples with M_S = 2.3, M_A = 1.5 and various BSF values, heated at 900 °C for 60 minutes

BSF (%)	Temperature (°C)	Heating Time (minutes)	Major Phase(s)	Minor Phase(s)
86	900	60	$BaCO_3$	$2BaO.SiO_2$ $BaO.SiO_2$ $3BaO.Al_2O_3$
90	900	60	$BaCO_3$	$2BaO.SiO_2$ $BaO.SiO_2$ $3BaO.Al_2O_3$
94	900	60	$BaCO_3$	$2BaO.SiO_2$ $BaO.SiO_2$ $3BaO.Al_2O_3$
98	900	60	$BaCO_3$	$2BaO.SiO_2$ $BaO.SiO_2$ $3BaO.Al_2O_3$
102	900	60	$BaCO_3$	$2BaO.SiO_2$ $BaO.SiO_2$ $3BaO.Al_2O_3$

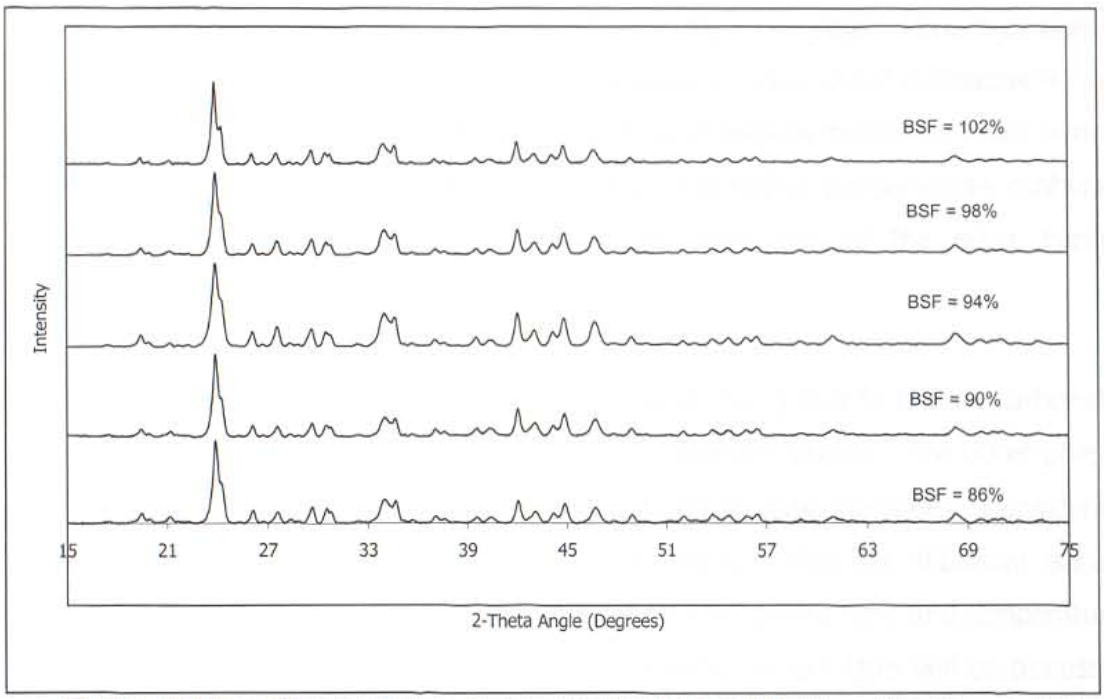

Figure 3.30: Diffractograms of quaternary samples with M_S = 2.3, M_A = 1.5 and various BSF values, heated at 900 °C for 60 minutes

3.6.1 The Quaternary System $BaO-Al_2O_3-Fe_2O_3-SiO_2$, with BSF = 86 %, M_S = 2.3 and M_A = 1.5

The diffractograms of the quaternary samples with BSF = 86 %, initially heated at 900 °C for 60 minutes and then at 1000, 1100, 1200, 1300 or 1400 °C for 15, 30, 60 or 120 minutes, are shown in Figures 3.31 to 3.35. Using Diffrac^{Plus} software and comparing the diffractograms with the reference patterns shown in Section 3.3.1, it was found that all samples contained mainly orthorhombic barium carbonate and orthorhombic dibarium silicate. Small quantities of orthorhombic monobarium silicate, hexagonal barium aluminium silicate ($BaO.Al_2O_3.SiO_2$), hexagonal monobarium aluminate, and cubic tribarium aluminate were also detected in most of the samples. In addition, various barium hydroxides were detected in some samples. The barium hydroxides detected included the normal barium hydroxide, $Ba(OH)_2$, the monohydrate, $Ba(OH)_2.H_2O$, the trihydrate, $Ba(OH)_2.3H_2O$, and the octahydrate, $Ba(OH)_2.8H_2O$.

No uncombined barium oxide was detected in any of the samples. It appeared that

the uncombined barium oxide had converted to the more stable barium carbonate and barium hydroxide forms (this will be discussed in more detail in Chapter 4). All samples appeared to contain bigger quantities of barium carbonate than barium hydroxide. Most samples heated for longer and at higher temperatures contained barium hydroxide octahydrate in combination with one of the other barium hydroxides.

In the diffractograms, the peak at 23.9 °2θ was primarily due to barium carbonate, while the peak at 29.6 °2θ was mainly due to dibarium silicate. The other phases present in the samples contributed very little to these peak intensities. Considering these two peaks in Figures 3.31 to 3.35, it appears that the dibarium silicate content in the samples increased with an increase in heating time and temperature, with a corresponding decrease in barium carbonate content (this will be discussed in more detail in Chapter 4). In the samples heated at 1300 and 1400 °C, the barium carbonate content seemed to vary irregularly with heating time. This could probably have been due to varying quantities of uncombined BaO being present in the form of the different barium hydroxides instead of barium carbonate.

Monobarium silicate was present in all samples except those heated for 120 minutes at 1300 °C or for 60 minutes or longer at 1400 °C.

Barium aluminium silicate was detected in the sample heated for 120 minutes at 1100 °C and in most samples that were heated at higher temperatures. In samples where both barium hydroxide monohydrate and barium hydroxide octahydrate were present, detection of barium aluminium silicate was very difficult due to extensive peak overlap of barium aluminium silicate with these two phases. It is possible that samples indicated to contain the monohydrate and octahydrate probably also contained barium aluminium silicate.

Monobarium aluminate was present in all samples heated at 1000 °C and in those heated for up to 30 minutes at the higher temperatures. Tribarium aluminate was detected in all samples except those heated for 120 minutes at 1300 °C or for 60

minutes or longer at 1400 °C.

The crystalline phases identified in the samples with BSF = 86 %, are listed in Tables 3.8 to 3.12. Descriptions of these phases are given in Table 3.2 and Appendix A. The distinction between major and minor phases in the tables depended on the relative peak intensities of the individual phases in the diffractograms. In general, the peaks in the diffractograms due to the minor phases, were too small to observe any trends of these phases with heating time or temperature.

Table 3.8: Crystalline phases identified in samples with M_S = 2.3, M_A = 1.5 and BSF = 86 %, heated at 900 °C for 60 minutes and then at 1000 °C for different time periods

BSF (%)	Temperature (°C)	Heating Time (minutes)	Major Phase(s)	Minor Phase(s)
86	1000	15	$BaCO_3$ $2BaO.SiO_2$	$BaO.SiO_2$ $BaO.Al_2O_3$ $3BaO.Al_2O_3$
86	1000	30	$BaCO_3$ $2BaO.SiO_2$	$BaO.SiO_2$ $BaO.Al_2O_3$ $3BaO.Al_2O_3$ $Ba(OH)_2.3H_2O$
86	1000	60	$BaCO_3$ $2BaO.SiO_2$	$BaO.SiO_2$ $BaO.Al_2O_3$ $3BaO.Al_2O_3$ $Ba(OH)_2$
86	1000	120	$BaCO_3$ $2BaO.SiO_2$	$BaO.SiO_2$ $BaO.Al_2O_3$ $3BaO.Al_2O_3$ $Ba(OH)_2$

Table 3.9: Crystalline phases identified in samples with M_S = 2.3, M_A = 1.5 and BSF = 86 %, heated at 900 °C for 60 minutes and then at 1100 °C for different time periods

BSF (%)	Temperature (°C)	Heating Time (minutes)	Major Phase(s)	Minor Phase(s)
86	1100	15	$BaCO_3$ $2BaO.SiO_2$	$BaO.SiO_2$ $BaO.Al_2O_3$ $3BaO.Al_2O_3$ $Ba(OH)_2$
86	1100	30	$BaCO_3$ $2BaO.SiO_2$	$BaO.SiO_2$ $3BaO.Al_2O_3$ $Ba(OH)_2$
86	1100	60	$BaCO_3$ $2BaO.SiO_2$	$BaO.SiO_2$ $3BaO.Al_2O_3$ $Ba(OH)_2.H_2O$ $Ba(OH)_2.8H_2O$
86	1100	120	$BaCO_3$ $2BaO.SiO_2$	$BaO.SiO_2$ $BaO.Al_2O_3.SiO_2$ $3BaO.Al_2O_3$ $Ba(OH)_2.H_2O$ $Ba(OH)_2.8H_2O$

Table 3.10: Crystalline phases identified in samples with M_S = 2.3, M_A = 1.5 and BSF = 86 %, heated at 900 °C for 60 minutes and then at 1200 °C for different time periods

BSF (%)	Temperature (°C)	Heating Time (minutes)	Major Phase(s)	Minor Phase(s)
86	1200	15	$BaCO_3$ $2BaO.SiO_2$	$BaO.SiO_2$ $BaO.Al_2O_3.SiO_2$ $BaO.Al_2O_3$ $3BaO.Al_2O_3$ $Ba(OH)_2$ $Ba(OH)_2.8H_2O$
86	1200	30	$BaCO_3$ $2BaO.SiO_2$	$BaO.SiO_2$ $BaO.Al_2O_3.SiO_2$ $BaO.Al_2O_3$ $3BaO.Al_2O_3$ $Ba(OH)_2.3H_2O$ $Ba(OH)_2.8H_2O$
86	1200	60	$BaCO_3$ $2BaO.SiO_2$	$BaO.SiO_2$ $BaO.Al_2O_3.SiO_2$ $BaO.Al_2O_3$ $3BaO.Al_2O_3$ $Ba(OH)_2.3H_2O$ $Ba(OH)_2.8H_2O$
86	1200	120	$BaCO_3$ $2BaO.SiO_2$	$BaO.SiO_2$ $BaO.Al_2O_3.SiO_2$ $3BaO.Al_2O_3$ $Ba(OH)_2.8H_2O$

Table 3.11: Crystalline phases identified in samples with M_S = 2.3, M_A = 1.5 and BSF = 86 %, heated at 900 °C for 60 minutes and then at 1300 °C for different time periods

BSF (%)	Temperature (°C)	Heating Time (minutes)	Major Phase(s)	Minor Phase(s)
86	1300	15	$BaCO_3$ $2BaO.SiO_2$	$BaO.SiO_2$ $BaO.Al_2O_3$ $3BaO.Al_2O_3$ $Ba(OH)_2.H_2O$ $Ba(OH)_2.3H_2O$ $Ba(OH)_2.8H_2O$
86	1300	30	$BaCO_3$ $2BaO.SiO_2$	$BaO.SiO_2$ $BaO.Al_2O_3.SiO_2$ $3BaO.Al_2O_3$ $Ba(OH)_2.3H_2O$ $Ba(OH)_2.8H_2O$
86	1300	60	$2BaO.SiO_2$	$BaCO_3$ $BaO.SiO_2$ $BaO.Al_2O_3.SiO_2$ $3BaO.Al_2O_3$ $Ba(OH)_2$ $Ba(OH)_2.8H_2O$
86	1300	120	$BaCO_3$ $2BaO.SiO_2$	$BaO.Al_2O_3.SiO_2$ $Ba(OH)_2$ $Ba(OH)_2.8H_2O$

Table 3.12: Crystalline phases identified in samples with M_S = 2.3, M_A = 1.5 and BSF = 86 %, heated at 900 °C for 60 minutes and then at 1400 °C for different time periods

BSF (%)	Temperature (°C)	Heating Time (minutes)	Major Phase(s)	Minor Phase(s)
86	1400	15	$2BaO.SiO_2$	$BaCO_3$ $BaO.SiO_2$ $BaO.Al_2O_3.SiO_2$ $BaO.Al_2O_3$ $3BaO.Al_2O_3$ $Ba(OH)_2$ $Ba(OH)_2.3H_2O$ $Ba(OH)_2.8H_2O$
86	1400	30	$BaCO_3$ $2BaO.SiO_2$	$BaO.SiO_2$ $BaO.Al_2O_3.SiO_2$ $3BaO.Al_2O_3$ $Ba(OH)_2.H_2O$ $Ba(OH)_2.8H_2O$
86	1400	60	$BaCO_3$ $2BaO.SiO_2$	$BaO.Al_2O_3.SiO_2$ $Ba(OH)_2$ $Ba(OH)_2.H_2O$ $Ba(OH)_2.8H_2O$
86	1400	120	$BaCO_3$ $2BaO.SiO_2$	$Ba(OH)_2$ $Ba(OH)_2.3H_2O$ $Ba(OH)_2.8H_2O$

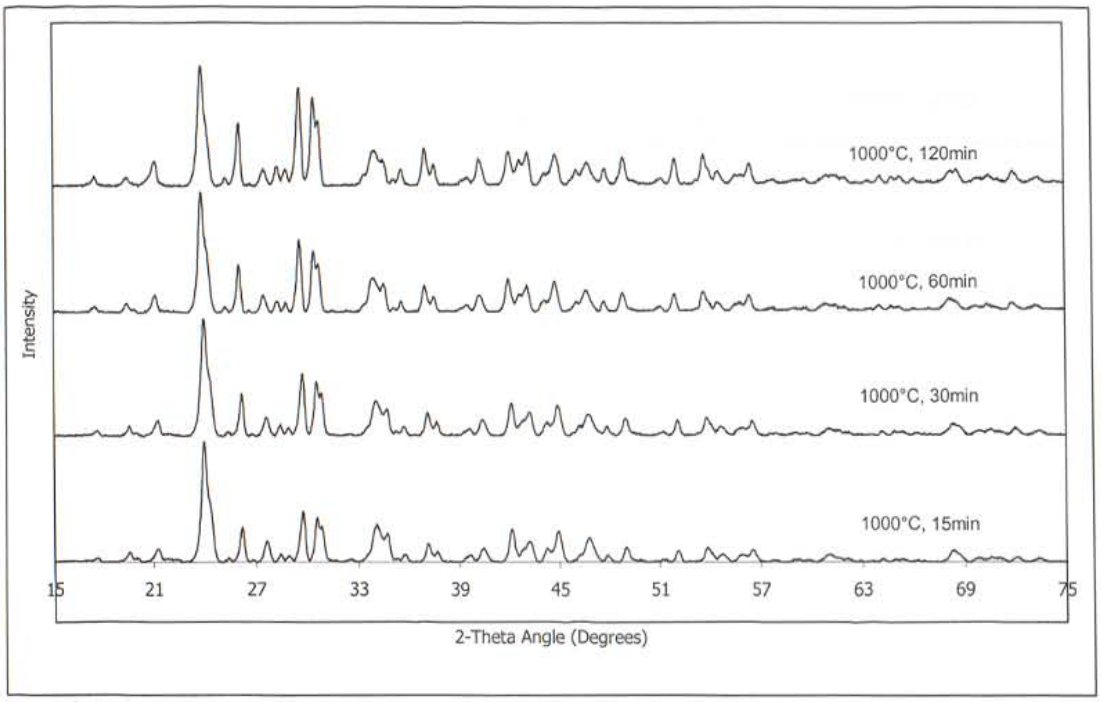

Figure 3.31: Diffractograms of quaternary samples with M_S = 2.3, M_A = 1.5 and BSF = 86 %, heated at 900 °C for 60 minutes and then at 1000 °C for different time periods

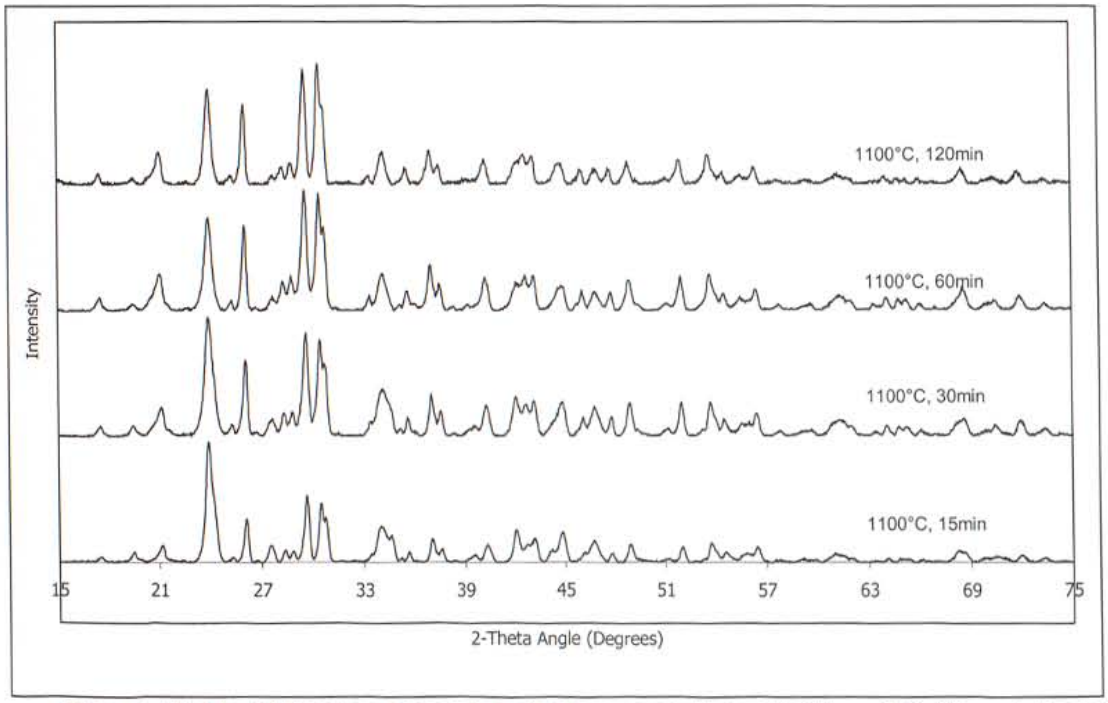

Figure 3.32: Diffractograms of quaternary samples with M_S = 2.3, M_A = 1.5 and BSF = 86 %, heated at 900 °C for 60 minutes and then at 1100 °C for different time periods

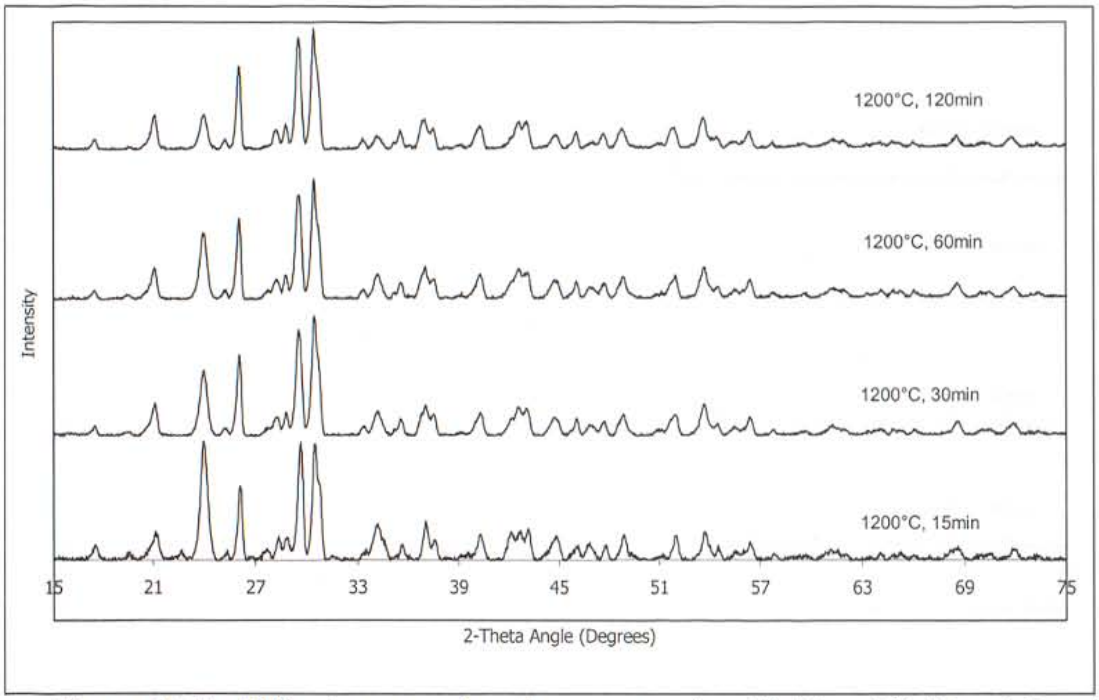

Figure 3.33: Diffractograms of quaternary samples with M_S = 2.3, M_A = 1.5 and BSF = 86 %, heated at 900 °C for 60 minutes and then at 1200 °C for different time periods

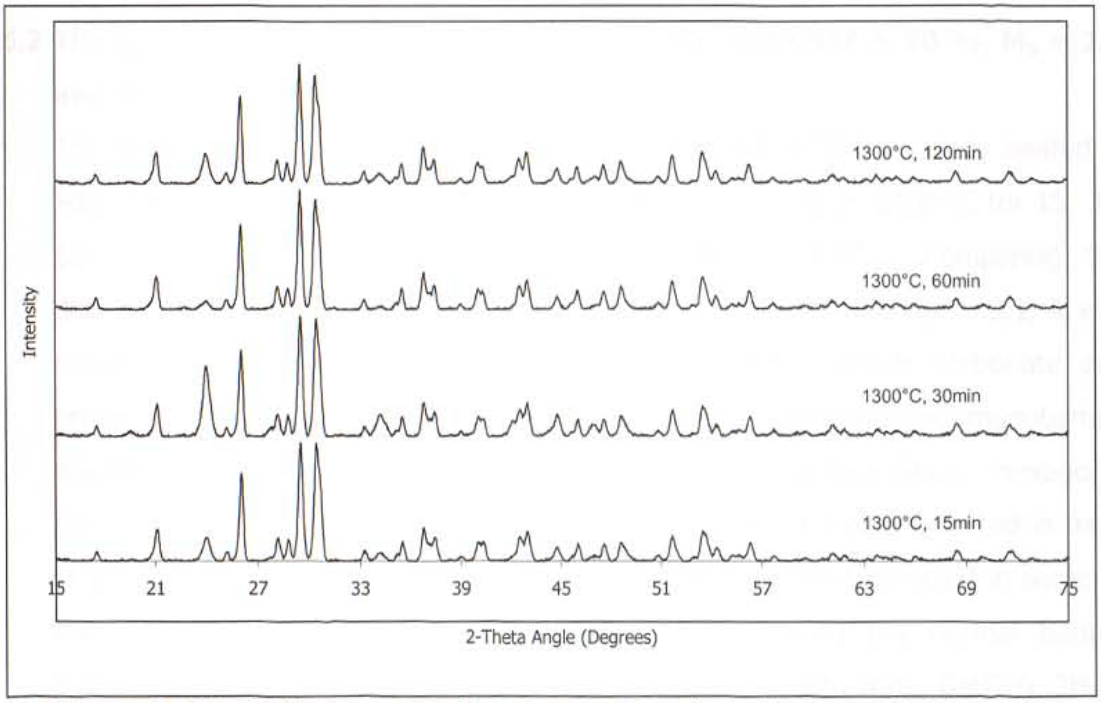

Figure 3.34: Diffractograms of quaternary samples with M_S = 2.3, M_A = 1.5 and BSF = 86 %, heated at 900 °C for 60 minutes and then at 1300 °C for different time periods

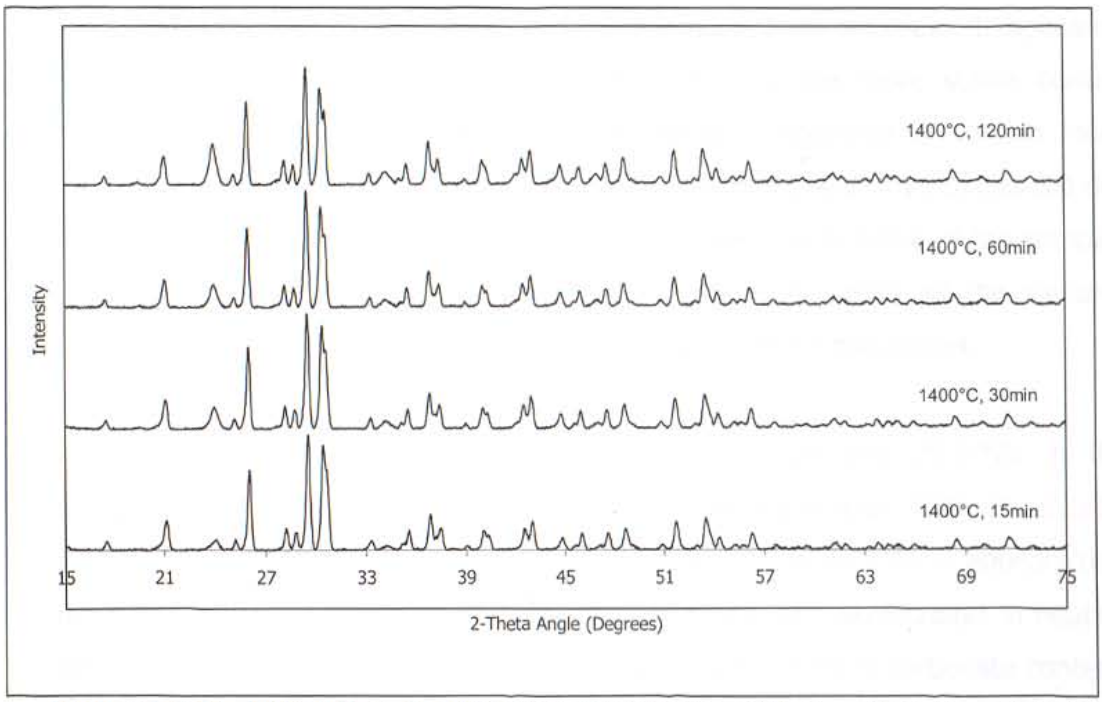

Figure 3.35: Diffractograms of quaternary samples with M_S = 2.3, M_A = 1.5 and BSF = 86 %, heated at 900 °C for 60 minutes and then at 1400 °C for different time periods

3.6.2 The Quaternary System $BaO-Al_2O_3-Fe_2O_3-SiO_2$, with BSF = 90 %, M_S = 2.3 and M_A = 1.5

The diffractograms of the quaternary samples with BSF = 90 %, initially heated at 900 °C for 60 minutes and then at 1000, 1100, 1200, 1300 or 1400 °C for 15, 30, 60 or 120 minutes, are shown in Figures 3.36 to 3.40. Comparing the diffractograms with the reference patterns that are shown in Section 3.3.1, it was found that all samples contained mainly orthorhombic barium carbonate and orthorhombic dibarium silicate. Small quantities of orthorhombic monobarium silicate, hexagonal barium aluminium silicate ($BaO.Al_2O_3.SiO_2$), hexagonal monobarium aluminate, and cubic tribarium aluminate were also detected in most of the samples. In addition, various barium hydroxides were detected in some of the samples. The barium hydroxides detected included the normal barium hydroxide, $Ba(OH)_2$, the monohydrate, $Ba(OH)_2.H_2O$, the trihydrate, $Ba(OH)_2.3H_2O$, and the octahydrate, $Ba(OH)_2.8H_2O$.

No uncombined barium oxide was detected in any of these samples. It appeared that the uncombined barium oxide had converted to the more stable barium carbonate and barium hydroxide forms. All samples appeared to contain more barium carbonate than barium hydroxide. The different barium hydroxides did not appear to occur in any particular order in the samples. Only some of the samples heated at 1000 to 1200 °C contained some hydroxides, while all the samples heated at 1300 and 1400 °C contained at least two different hydroxides.

As mentioned in Section 3.6.1, the peaks at 23.9 °2θ and 29.6 °2θ in the diffractograms were primarily due to barium carbonate and dibarium silicate, respectively. Considering these two peaks in Figures 3.36 to 3.40, it appears that the dibarium silicate content in the samples increased with an increase in heating time and temperature, with a corresponding decrease in barium carbonate content. Similarly to the samples with BSF = 86 %, the barium carbonate content seemed to vary irregularly with heating time in samples heated at 1300 and 1400 °C. This could probably have been because of varying quantities of uncombined BaO being present in the form of the different barium hydroxides instead of barium carbonate.

Monobarium silicate was present in most samples. The samples heated for longer than 15 minutes at 1400 °C did not contain any monobarium silicate.

Barium aluminium silicate was detected in some of the samples heated at 1100 to 1200 °C and in most samples heated at higher temperatures. As previously, in samples where both barium hydroxide monohydrate and barium hydroxide octahydrate were present, detection of barium aluminium silicate was very difficult due to extensive peak overlap of barium aluminium silicate with these two phases. It is therefore possible that samples indicated to contain the monohydrate and octahydrate probably also contained barium aluminium silicate.

Monobarium aluminate was present in most samples heated in the temperature range 1000 to 1400 °C, but samples heated for longer than 30 to 60 minutes at a specific temperature did not contain monobarium aluminate. Tribarium aluminate

was detected in all samples except those heated for 30 minutes or longer at 1400 °C.

The crystalline phases identified in the samples with BSF = 90 %, are listed in Tables 3.13 to 3.17. Descriptions of these phases are given in Table 3.2 and Appendix A. The distinction between major and minor phases in the tables depended on the relative peak intensities of the individual phases in the diffractograms. The peaks in the diffractograms due to the minor phases were, in general, too small to observe any trends of these phases with heating time or temperature.

Table 3.13: Crystalline phases identified in samples with M_S = 2.3, M_A = 1.5 and BSF = 90 %, heated at 900 °C for 60 minutes and then at 1000 °C for different time periods

BSF (%)	Temperature (°C)	Heating Time (minutes)	Major Phase(s)	Minor Phase(s)
90	1000	15	$BaCO_3$ $2BaO.SiO_2$	$BaO.SiO_2$ $BaO.Al_2O_3$ $3BaO.Al_2O_3$
90	1000	30	$BaCO_3$ $2BaO.SiO_2$	$BaO.SiO_2$ $BaO.Al_2O_3$ $3BaO.Al_2O_3$ $Ba(OH)_2$
90	1000	60	$BaCO_3$ $2BaO.SiO_2$	$BaO.SiO_2$ $3BaO.Al_2O_3$
90	1000	120	$BaCO_3$ $2BaO.SiO_2$	$BaO.SiO_2$ $3BaO.Al_2O_3$

Table 3.14: Crystalline phases identified in samples with M_S = 2.3, M_A = 1.5 and BSF = 90 %, heated at 900 °C for 60 minutes and then at 1100 °C for different time periods

BSF (%)	Temperature (°C)	Heating Time (minutes)	Major Phase(s)	Minor Phase(s)
90	1100	15	$BaCO_3$ $2BaO.SiO_2$	$BaO.SiO_2$ $BaO.Al_2O_3.SiO_2$ $BaO.Al_2O_3$ $3BaO.Al_2O_3$
90	1100	30	$BaCO_3$ $2BaO.SiO_2$	$BaO.SiO_2$ $BaO.Al_2O_3.SiO_2$ $BaO.Al_2O_3$ $3BaO.Al_2O_3$
90	1100	60	$BaCO_3$ $2BaO.SiO_2$	$BaO.SiO_2$ $BaO.Al_2O_3.SiO_2$ $3BaO.Al_2O_3$ $Ba(OH)_2$
90	1100	120	$BaCO_3$ $2BaO.SiO_2$	$BaO.Al_2O_3.SiO_2$ $3BaO.Al_2O_3$ $Ba(OH)_2.H_2O$ $Ba(OH)_2.8H_2O$

Table 3.15: Crystalline phases identified in samples with M_S = 2.3, M_A = 1.5 and BSF = 90 %, heated at 900 °C for 60 minutes and then at 1200 °C for different time periods

BSF (%)	Temperature (°C)	Heating Time (minutes)	Major Phase(s)	Minor Phase(s)
90	1200	15	$BaCO_3$ $2BaO.SiO_2$	$BaO.SiO_2$ $BaO.Al_2O_3$ $3BaO.Al_2O_3$ $Ba(OH)_2$
90	1200	30	$BaCO_3$ $2BaO.SiO_2$	$BaO.SiO_2$ $BaO.Al_2O_3$ $3BaO.Al_2O_3$ $Ba(OH)_2.8H_2O$
90	1200	60	$BaCO_3$ $2BaO.SiO_2$	$BaO.SiO_2$ $BaO.Al_2O_3$ $3BaO.Al_2O_3$ $Ba(OH)_2.3H_2O$ $Ba(OH)_2.8H_2O$
90	1200	120	$BaCO_3$ $2BaO.SiO_2$	$BaO.SiO_2$ $BaO.Al_2O_3.SiO_2$ $3BaO.Al_2O_3$ $Ba(OH)_2.8H_2O$

Table 3.16: Crystalline phases identified in samples with M_S = 2.3, M_A = 1.5 and BSF = 90 %, heated at 900 °C for 60 minutes and then at 1300 °C for different time periods

BSF (%)	Temperature (°C)	Heating Time (minutes)	Major Phase(s)	Minor Phase(s)
90	1300	15	$BaCO_3$ $2BaO.SiO_2$	$BaO.SiO_2$ $BaO.Al_2O_3$ $3BaO.Al_2O_3$ $Ba(OH)_2.H_2O$ $Ba(OH)_2.3H_2O$ $Ba(OH)_2.8H_2O$
90	1300	30	$BaCO_3$ $2BaO.SiO_2$	$BaO.SiO_2$ $BaO.Al_2O_3.SiO_2$ $BaO.Al_2O_3$ $3BaO.Al_2O_3$ $Ba(OH)_2.3H_2O$ $Ba(OH)_2.8H_2O$
90	1300	60	$BaCO_3$ $2BaO.SiO_2$	$BaO.SiO_2$ $BaO.Al_2O_3.SiO_2$ $BaO.Al_2O_3$ $3BaO.Al_2O_3$ $Ba(OH)_2$ $Ba(OH)_2.H_2O$ $Ba(OH)_2.3H_2O$
90	1300	120	$BaCO_3$ $2BaO.SiO_2$	$BaO.SiO_2$ $BaO.Al_2O_3.SiO_2$ $3BaO.Al_2O_3$ $Ba(OH)_2$ $Ba(OH)_2.3H_2O$

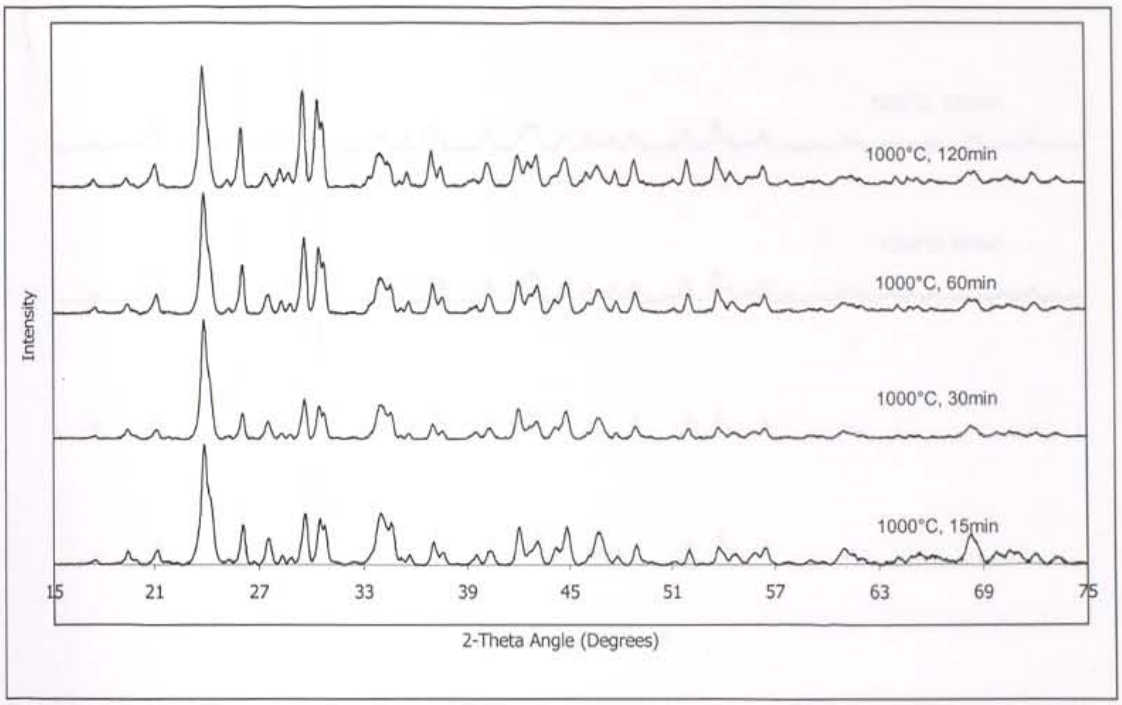

Figure 3.36: Diffractograms of quaternary samples with M_S = 2.3, M_A = 1.5 and BSF = 90 %, heated at 900 °C for 60 minutes and then at 1000 °C for different time periods

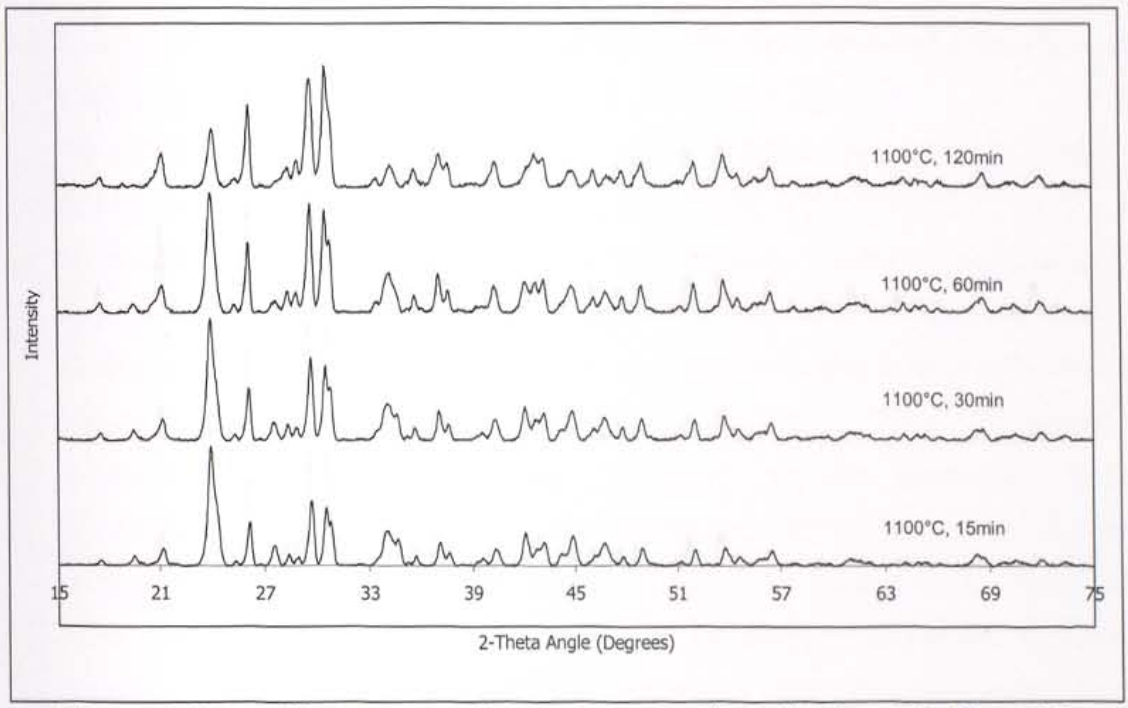

Figure 3.37: Diffractograms of quaternary samples with M_S = 2.3, M_A = 1.5 and BSF = 90 %, heated at 900 °C for 60 minutes and then at 1100 °C for different time periods

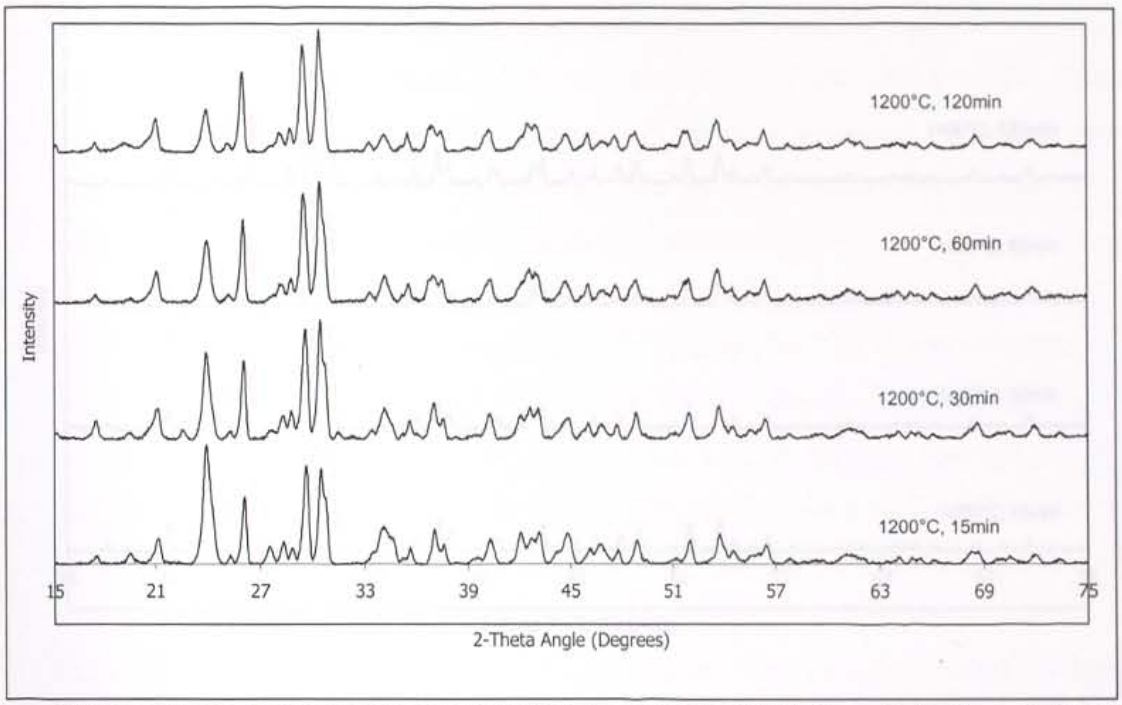

Figure 3.38: Diffractograms of quaternary samples with M_S = 2.3, M_A = 1.5 and BSF = 90 %, heated at 900 °C for 60 minutes and then at 1200 °C for different time periods

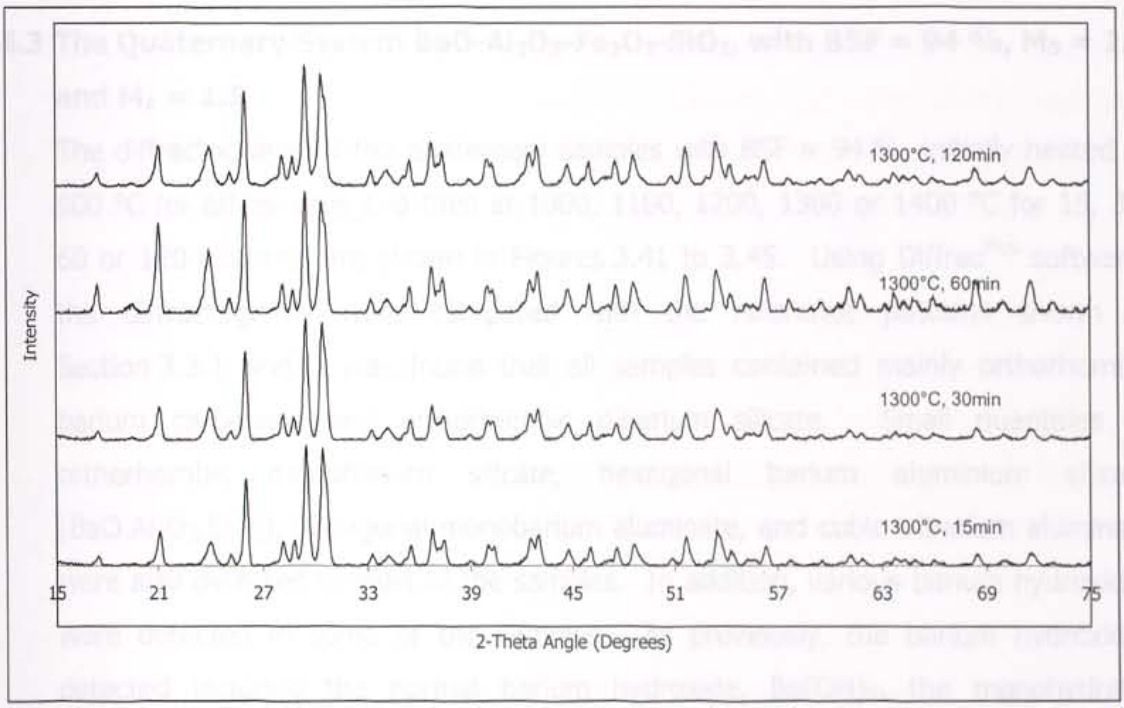

Figure 3.39: Diffractograms of quaternary samples with M_S = 2.3, M_A = 1.5 and BSF = 90 %, heated at 900 °C for 60 minutes and then at 1300 °C for different time periods

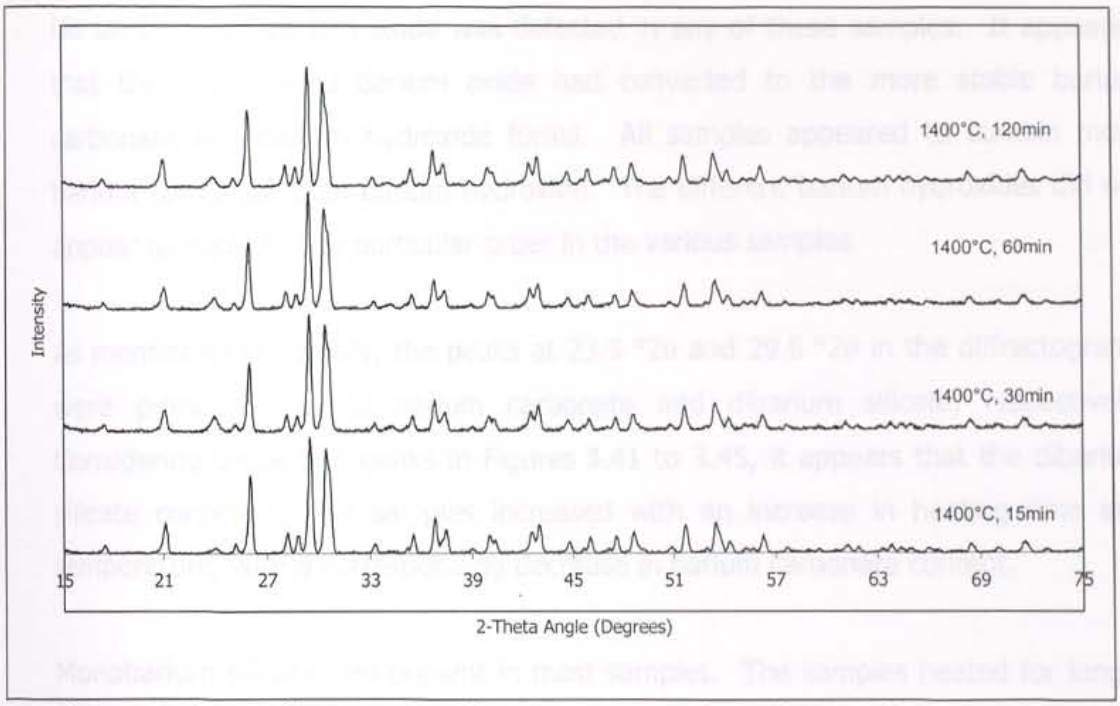

Figure 3.40: Diffractograms of quaternary samples with M_S = 2.3, M_A = 1.5 and BSF = 90 %, heated at 900 °C for 60 minutes and then at 1400 °C for different time periods

3.6.3 The Quaternary System BaO-Al_2O_3-Fe_2O_3-SiO_2, with BSF = 94 %, M_S = 2.3 and M_A = 1.5

The diffractograms of the quaternary samples with BSF = 94 %, initially heated at 900 °C for 60 minutes and then at 1000, 1100, 1200, 1300 or 1400 °C for 15, 30, 60 or 120 minutes, are shown in Figures 3.41 to 3.45. Using Diffrac^{Plus} software, the diffractograms were compared with the reference patterns shown in Section 3.3.1 and it was found that all samples contained mainly orthorhombic barium carbonate and orthorhombic dibarium silicate. Small quantities of orthorhombic monobarium silicate, hexagonal barium aluminium silicate ($BaO.Al_2O_3.SiO_2$), hexagonal monobarium aluminate, and cubic tribarium aluminate were also detected in most of the samples. In addition, various barium hydroxides were detected in some of the samples. As previously, the barium hydroxides detected included the normal barium hydroxide, $Ba(OH)_2$, the monohydrate, $Ba(OH)_2.H_2O$, the trihydrate, $Ba(OH)_2.3H_2O$, and the octahydrate, $Ba(OH)_2.8H_2O$.

No uncombined barium oxide was detected in any of these samples. It appeared that the uncombined barium oxide had converted to the more stable barium carbonate and barium hydroxide forms. All samples appeared to contain more barium carbonate than barium hydroxide. The different barium hydroxides did not appear to occur in any particular order in the various samples.

As mentioned previously, the peaks at 23.9 °2θ and 29.6 °2θ in the diffractograms were primarily due to barium carbonate and dibarium silicate, respectively. Considering these two peaks in Figures 3.41 to 3.45, it appears that the dibarium silicate content in the samples increased with an increase in heating time and temperature, with a corresponding decrease in barium carbonate content.

Monobarium silicate was present in most samples. The samples heated for longer than 15 minutes at 1400 °C did not contain any monobarium silicate.

Barium aluminium silicate was detected in most samples heated at 1100 to 1300 °C. It is possible that the samples heated at 1400 °C that contained both barium hydroxide monohydrate and barium hydroxide octahydrate, also contained barium aluminium silicate. The detection of barium aluminium silicate was very difficult in samples containing both the monohydrate and the octahydrate due to extensive peak overlap of barium aluminium silicate with these two phases.

Monobarium aluminate was present in only some samples heated in the temperature range 1000 to 1400 °C. In general, samples heated for longer than 30 to 60 minutes at a specific temperature did not contain monobarium aluminate. Tribarium aluminate was detected in all samples except those heated for longer at 1300 and 1400 °C.

The crystalline phases identified in the samples with BSF = 94 %, are listed in Tables 3.18 to 3.22. Descriptions of these phases are given in Table 3.2 and Appendix A. The distinction between major and minor phases in the tables depended on the relative peak intensities of the individual phases in the

diffractograms. The peaks in the diffractograms due to the minor phases were, in general, too small to observe any trends of these phases with heating time or temperature.

Table 3.18: Crystalline phases identified in samples with M_S = 2.3, M_A = 1.5 and BSF = 94 %, heated at 900 °C for 60 minutes and then at 1000 °C for different time periods

BSF (%)	Temperature (°C)	Heating Time (minutes)	Major Phase(s)	Minor Phase(s)
94	1000	15	$BaCO_3$ $2BaO.SiO_2$	$BaO.SiO_2$ $BaO.Al_2O_3$ $3BaO.Al_2O_3$
94	1000	30	$BaCO_3$ $2BaO.SiO_2$	$BaO.SiO_2$ $BaO.Al_2O_3$ $3BaO.Al_2O_3$
94	1000	60	$BaCO_3$ $2BaO.SiO_2$	$BaO.SiO_2$ $BaO.Al_2O_3$ $3BaO.Al_2O_3$ $Ba(OH)_2$
94	1000	120	$BaCO_3$ $2BaO.SiO_2$	$BaO.SiO_2$ $3BaO.Al_2O_3$ $Ba(OH)_2$

Table 3.19: Crystalline phases identified in samples with M_S = 2.3, M_A = 1.5 and BSF = 94 %, heated at 900 °C for 60 minutes and then at 1100 °C for different time periods

BSF (%)	Temperature (°C)	Heating Time (minutes)	Major Phase(s)	Minor Phase(s)
94	1100	15	$BaCO_3$ $2BaO.SiO_2$	$BaO.SiO_2$ $BaO.Al_2O_3.SiO_2$ $BaO.Al_2O_3$ $3BaO.Al_2O_3$
94	1100	30	$BaCO_3$ $2BaO.SiO_2$	$BaO.SiO_2$ $BaO.Al_2O_3.SiO_2$ $3BaO.Al_2O_3$ $Ba(OH)_2$
94	1100	60	$BaCO_3$ $2BaO.SiO_2$	$BaO.SiO_2$ $BaO.Al_2O_3.SiO_2$ $3BaO.Al_2O_3$
94	1100	120	$BaCO_3$ $2BaO.SiO_2$	$BaO.SiO_2$ $BaO.Al_2O_3.SiO_2$ $3BaO.Al_2O_3$ $Ba(OH)_2.H_2O$ $Ba(OH)_2.8H_2O$

Table 3.20: Crystalline phases identified in samples with M_S = 2.3, M_A = 1.5 and BSF = 94 %, heated at 900 °C for 60 minutes and then at 1200 °C for different time periods

BSF (%)	Temperature (°C)	Heating Time (minutes)	Major Phase(s)	Minor Phase(s)
94	1200	15	$BaCO_3$ $2BaO.SiO_2$	$BaO.SiO_2$ $BaO.Al_2O_3$ $3BaO.Al_2O_3$
94	1200	30	$BaCO_3$ $2BaO.SiO_2$	$BaO.SiO_2$ $BaO.Al_2O_3$ $3BaO.Al_2O_3$ $Ba(OH)_2$
94	1200	60	$BaCO_3$ $2BaO.SiO_2$	$BaO.SiO_2$ $BaO.Al_2O_3.SiO_2$ $3BaO.Al_2O_3$ $Ba(OH)_2$ $Ba(OH)_2.8H_2O$
94	1200	120	$BaCO_3$ $2BaO.SiO_2$	$BaO.Al_2O_3.SiO_2$ $3BaO.Al_2O_3$ $Ba(OH)_2.3H_2O$ $Ba(OH)_2.8H_2O$

Table 3.21: Crystalline phases identified in samples with M_S = 2.3, M_A = 1.5 and BSF = 94 %, heated at 900 °C for 60 minutes and then at 1300 °C for different time periods

BSF (%)	Temperature (°C)	Heating Time (minutes)	Major Phase(s)	Minor Phase(s)
94	1300	15	$BaCO_3$ $2BaO.SiO_2$	$BaO.SiO_2$ $BaO.Al_2O_3.SiO_2$ $BaO.Al_2O_3$ $3BaO.Al_2O_3$ $Ba(OH)_2.H_2O$
94	1300	30	$BaCO_3$ $2BaO.SiO_2$	$BaO.SiO_2$ $BaO.Al_2O_3.SiO_2$ $Ba(OH)_2.8H_2O$
94	1300	60	$BaCO_3$ $2BaO.SiO_2$	$BaO.SiO_2$ $BaO.Al_2O_3.SiO_2$ $Ba(OH)_2$ $Ba(OH)_2.H_2O$ $Ba(OH)_2.8H_2O$
94	1300	120	$BaCO_3$ $2BaO.SiO_2$	$BaO.SiO_2$ $BaO.Al_2O_3.SiO_2$ $Ba(OH)_2.8H_2O$

Table 3.22: Crystalline phases identified in samples with M_S = 2.3, M_A = 1.5 and BSF = 94 %, heated at 900 °C for 60 minutes and then at 1400 °C for different time periods

BSF (%)	Temperature (°C)	Heating Time (minutes)	Major Phase(s)	Minor Phase(s)
94	1400	15	$BaCO_3$ $2BaO.SiO_2$	$BaO.SiO_2$ $BaO.Al_2O_3$ $3BaO.Al_2O_3$ $Ba(OH)_2.H_2O$
94	1400	30	$BaCO_3$ $2BaO.SiO_2$	$BaO.Al_2O_3$ $3BaO.Al_2O_3$ $Ba(OH)_2.H_2O$ $Ba(OH)_2.8H_2O$
94	1400	60	$BaCO_3$ $2BaO.SiO_2$	$3BaO.Al_2O_3$ $Ba(OH)_2.H_2O$ $Ba(OH)_2.8H_2O$
94	1400	120	$BaCO_3$ $2BaO.SiO_2$	$Ba(OH)_2.H_2O$ $Ba(OH)_2.8H_2O$

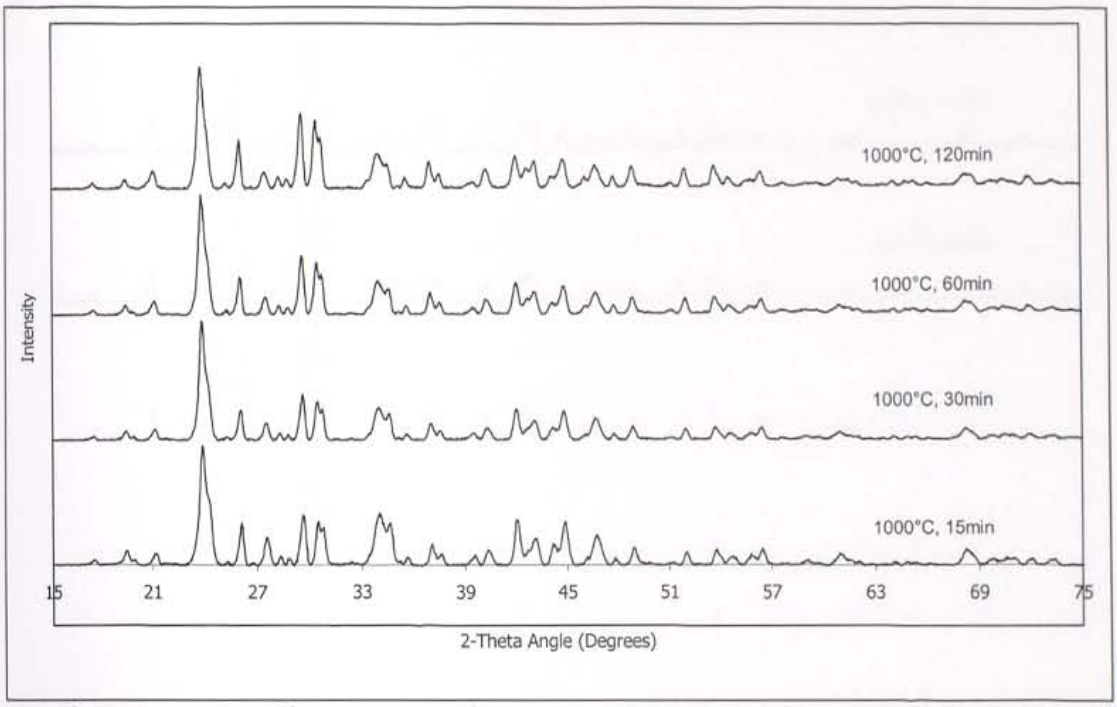

Figure 3.41: Diffractograms of quaternary samples with M_S = 2.3, M_A = 1.5 and BSF = 94 %, heated at 900 °C for 60 minutes and then at 1000 °C for different time periods

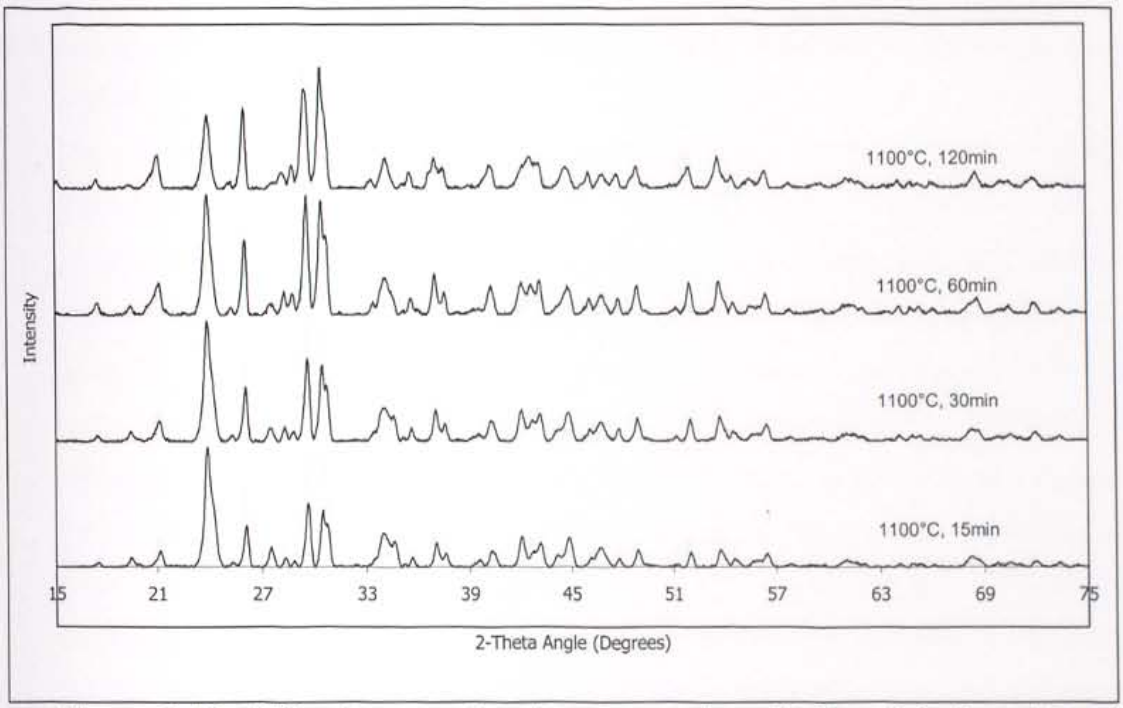

Figure 3.42: Diffractograms of quaternary samples with M_S = 2.3, M_A = 1.5 and BSF = 94 %, heated at 900 °C for 60 minutes and then at 1100 °C for different time periods

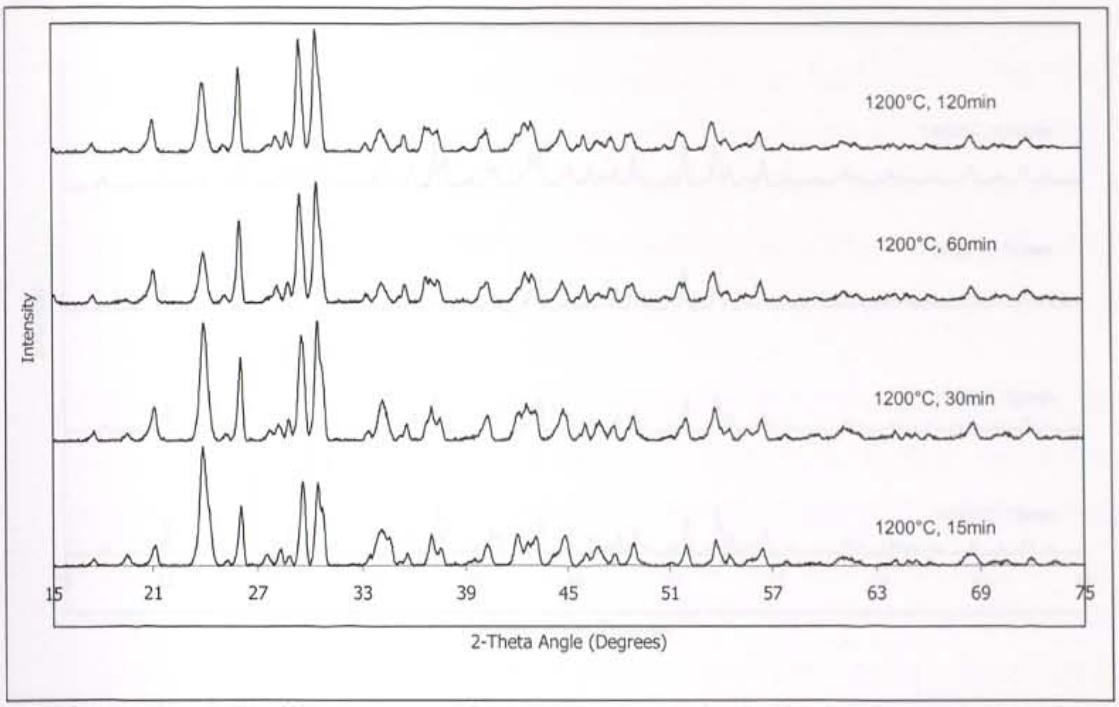

Figure 3.43: Diffractograms of quaternary samples with M_S = 2.3, M_A = 1.5 and BSF = 94 %, heated at 900 °C for 60 minutes and then at 1200 °C for different time periods

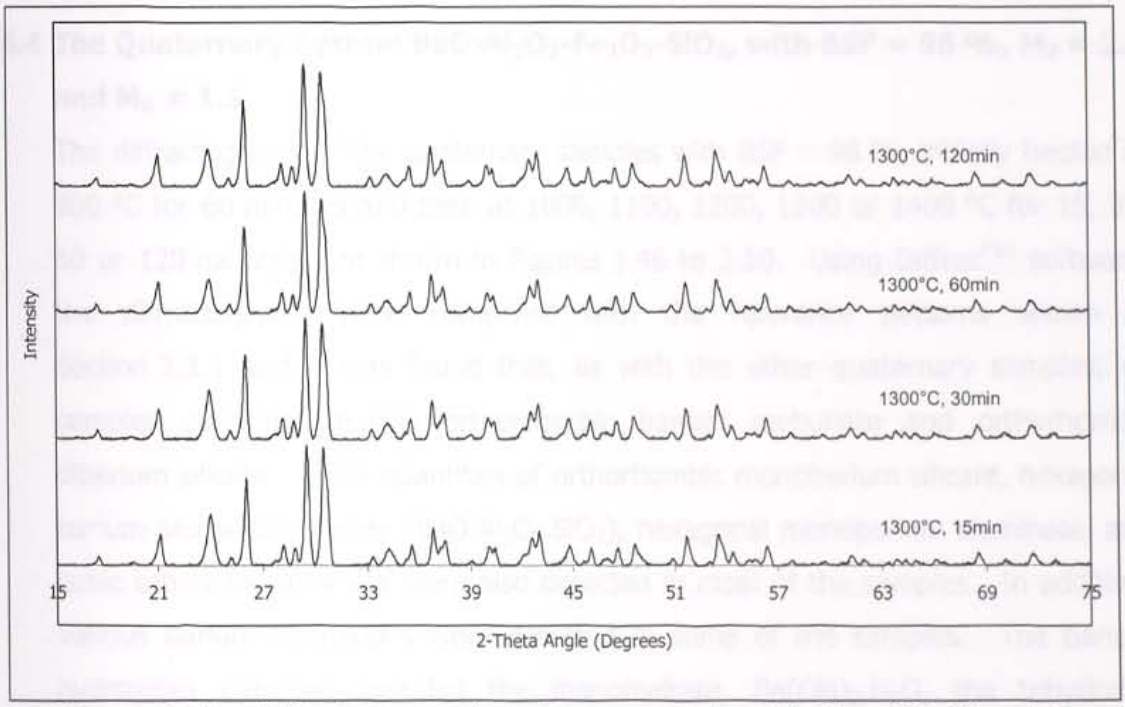

Figure 3.44: Diffractograms of quaternary samples with M_S = 2.3, M_A = 1.5 and BSF = 94 %, heated at 900 °C for 60 minutes and then at 1300 °C for different time periods

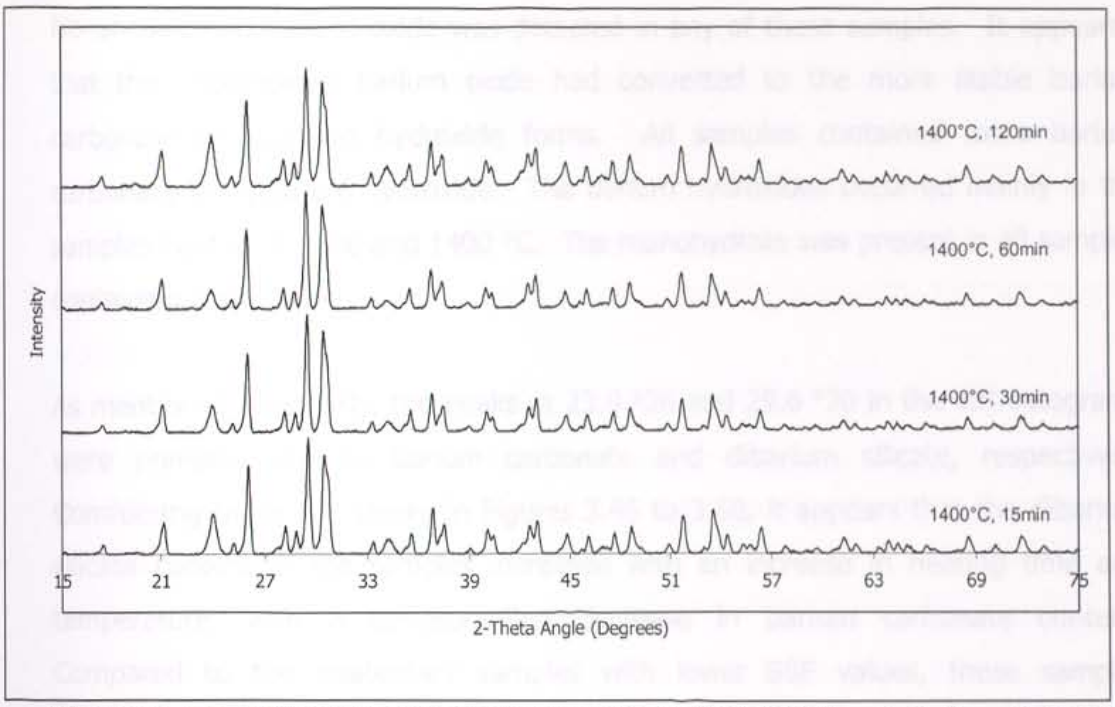

Figure 3.45: Diffractograms of quaternary samples with M_S = 2.3, M_A = 1.5 and BSF = 94 %, heated at 900 °C for 60 minutes and then at 1400 °C for different time periods

3.6.4 The Quaternary System BaO-Al_2O_3-Fe_2O_3-SiO_2, with BSF = 98 %, M_S = 2.3 and M_A = 1.5

The diffractograms of the quaternary samples with BSF = 98 %, initially heated at 900 °C for 60 minutes and then at 1000, 1100, 1200, 1300 or 1400 °C for 15, 30, 60 or 120 minutes, are shown in Figures 3.46 to 3.50. Using Diffrac^{Plus} software, the diffractograms were compared with the reference patterns shown in Section 3.3.1 and it was found that, as with the other quaternary samples, all samples contained mainly orthorhombic barium carbonate and orthorhombic dibarium silicate. Small quantities of orthorhombic monobarium silicate, hexagonal barium aluminium silicate ($BaO.Al_2O_3.SiO_2$), hexagonal monobarium aluminate, and cubic tribarium aluminate were also detected in most of the samples. In addition, various barium hydroxides were detected in some of the samples. The barium hydroxides detected included the monohydrate, $Ba(OH)_2.H_2O$, the trihydrate, $Ba(OH)_2.3H_2O$, and the octahydrate, $Ba(OH)_2.8H_2O$.

No uncombined barium oxide was detected in any of these samples. It appeared that the uncombined barium oxide had converted to the more stable barium carbonate and barium hydroxide forms. All samples contained more barium carbonate than barium hydroxide. The barium hydroxides occurred mainly in the samples heated at 1300 and 1400 °C. The monohydrate was present in all samples containing hydroxides.

As mentioned previously, the peaks at 23.9 °2θ and 29.6 °2θ in the diffractograms were primarily due to barium carbonate and dibarium silicate, respectively. Considering these two peaks in Figures 3.46 to 3.50, it appears that the dibarium silicate content in the samples increased with an increase in heating time and temperature, with a corresponding decrease in barium carbonate content. Compared to the quaternary samples with lower BSF values, these samples appeared to contain bigger fractions of uncombined BaO (in the form of barium carbonate) at a specific temperature.

Monobarium silicate was present in most samples. The sample heated for 120 minutes at 1200 °C and the samples heated for longer than 30 minutes at 1300 or 1400 °C did not contain any monobarium silicate.

Barium aluminium silicate was detected in some samples heated at 1100 to 1300 °C. It is possible that the sample heated for 60 minutes at 1400 °C that contained both barium hydroxide monohydrate and barium hydroxide octahydrate, also contained barium aluminium silicate. As already discussed, the detection of barium aluminium silicate was very difficult in samples containing both the monohydrate and the octahydrate.

Monobarium aluminate was only present in samples heated in the temperature range 1000 to 1200 °C. The samples heated for longer in this temperature range did not contain monobarium aluminate. Tribarium aluminate was present in all samples except those heated at 1300 and 1400 °C.

The crystalline phases identified in the samples with BSF = 98 %, are listed in Tables 3.23 to 3.27. Descriptions of these phases are given in Table 3.2 and Appendix A. The distinction between major and minor phases in the tables depended on the relative peak intensities of the individual phases in the diffractograms. The peaks in the diffractograms due to the minor phases were, in general, too small to observe any trends of these phases with heating time or temperature.

Table 3.23: Crystalline phases identified in samples with M_S = 2.3, M_A = 1.5 and BSF = 98 %, heated at 900 °C for 60 minutes and then at 1000 °C for different time periods

BSF (%)	Temperature (°C)	Heating Time (minutes)	Major Phase(s)	Minor Phase(s)
98	1000	15	$BaCO_3$ $2BaO.SiO_2$	$BaO.SiO_2$ $BaO.Al_2O_3$ $3BaO.Al_2O_3$
98	1000	30	$BaCO_3$ $2BaO.SiO_2$	$BaO.SiO_2$ $BaO.Al_2O_3$ $3BaO.Al_2O_3$
98	1000	60	$BaCO_3$ $2BaO.SiO_2$	$BaO.SiO_2$ $BaO.Al_2O_3$ $3BaO.Al_2O_3$
98	1000	120	$BaCO_3$ $2BaO.SiO_2$	$BaO.SiO_2$ $3BaO.Al_2O_3$

Table 3.24: Crystalline phases identified in samples with M_S = 2.3, M_A = 1.5 and BSF = 98 %, heated at 900 °C for 60 minutes and then at 1100 °C for different time periods

BSF (%)	Temperature (°C)	Heating Time (minutes)	Major Phase(s)	Minor Phase(s)
98	1100	15	$BaCO_3$ $2BaO.SiO_2$	$BaO.SiO_2$ $BaO.Al_2O_3$ $3BaO.Al_2O_3$
98	1100	30	$BaCO_3$ $2BaO.SiO_2$	$BaO.SiO_2$ $BaO.Al_2O_3.SiO_2$ $3BaO.Al_2O_3$
98	1100	60	$BaCO_3$ $2BaO.SiO_2$	$BaO.SiO_2$ $BaO.Al_2O_3.SiO_2$ $3BaO.Al_2O_3$
98	1100	120	$BaCO_3$ $2BaO.SiO_2$	$BaO.SiO_2$ $BaO.Al_2O_3.SiO_2$ $3BaO.Al_2O_3$ $Ba(OH)_2.H_2O$

Table 3.25: Crystalline phases identified in samples with M_S = 2.3, M_A = 1.5 and BSF = 98 %, heated at 900 °C for 60 minutes and then at 1200 °C for different time periods

BSF (%)	Temperature (°C)	Heating Time (minutes)	Major Phase(s)	Minor Phase(s)
98	1200	15	$BaCO_3$ $2BaO.SiO_2$	$BaO.SiO_2$ $BaO.Al_2O_3$ $3BaO.Al_2O_3$
98	1200	30	$BaCO_3$ $2BaO.SiO_2$	$BaO.SiO_2$ $BaO.Al_2O_3.SiO_2$ $BaO.Al_2O_3$ $3BaO.Al_2O_3$
98	1200	60	$BaCO_3$ $2BaO.SiO_2$	$BaO.SiO_2$ $BaO.Al_2O_3.SiO_2$ $3BaO.Al_2O_3$ $Ba(OH)_2.H_2O$
98	1200	120	$BaCO_3$ $2BaO.SiO_2$	$3BaO.Al_2O_3$ $Ba(OH)_2.H_2O$ $Ba(OH)_2.3H_2O$

Table 3.26: Crystalline phases identified in samples with M_S = 2.3, M_A = 1.5 and BSF = 98 %, heated at 900 °C for 60 minutes and then at 1300 °C for different time periods

BSF (%)	Temperature (°C)	Heating Time (minutes)	Major Phase(s)	Minor Phase(s)
98	1300	15	$BaCO_3$ $2BaO.SiO_2$	$BaO.SiO_2$
98	1300	30	$BaCO_3$ $2BaO.SiO_2$	$BaO.SiO_2$ $Ba(OH)_2.H_2O$ $Ba(OH)_2.3H_2O$
98	1300	60	$BaCO_3$ $2BaO.SiO_2$	$BaO.Al_2O_3.SiO_2$ $Ba(OH)_2.H_2O$
98	1300	120	$BaCO_3$ $2BaO.SiO_2$	$BaO.Al_2O_3.SiO_2$ $Ba(OH)_2.H_2O$

Table 3.27: Crystalline phases identified in samples with M_S = 2.3, M_A = 1.5 and BSF = 98 %, heated at 900 °C for 60 minutes and then at 1400 °C for different time periods

BSF (%)	Temperature (°C)	Heating Time (minutes)	Major Phase(s)	Minor Phase(s)
98	1400	15	$BaCO_3$ $2BaO.SiO_2$	$BaO.SiO_2$ $Ba(OH)_2.H_2O$
98	1400	30	$BaCO_3$ $2BaO.SiO_2$	$BaO.SiO_2$ $Ba(OH)_2.H_2O$
98	1400	60	$BaCO_3$ $2BaO.SiO_2$	$Ba(OH)_2.H_2O$ $Ba(OH)_2.8H_2O$
98	1400	120	$BaCO_3$ $2BaO.SiO_2$	$Ba(OH)_2.H_2O$

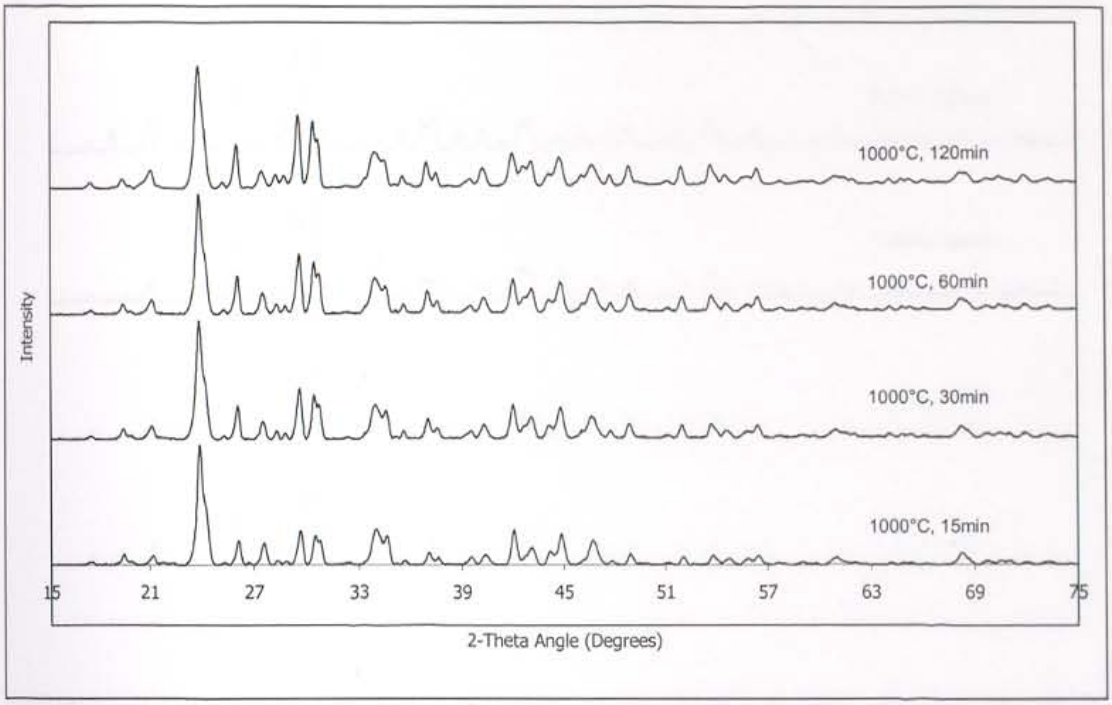

Figure 3.46: Diffractograms of quaternary samples with M_S = 2.3, M_A = 1.5 and BSF = 98 %, heated at 900 °C for 60 minutes and then at 1000 °C for different time periods

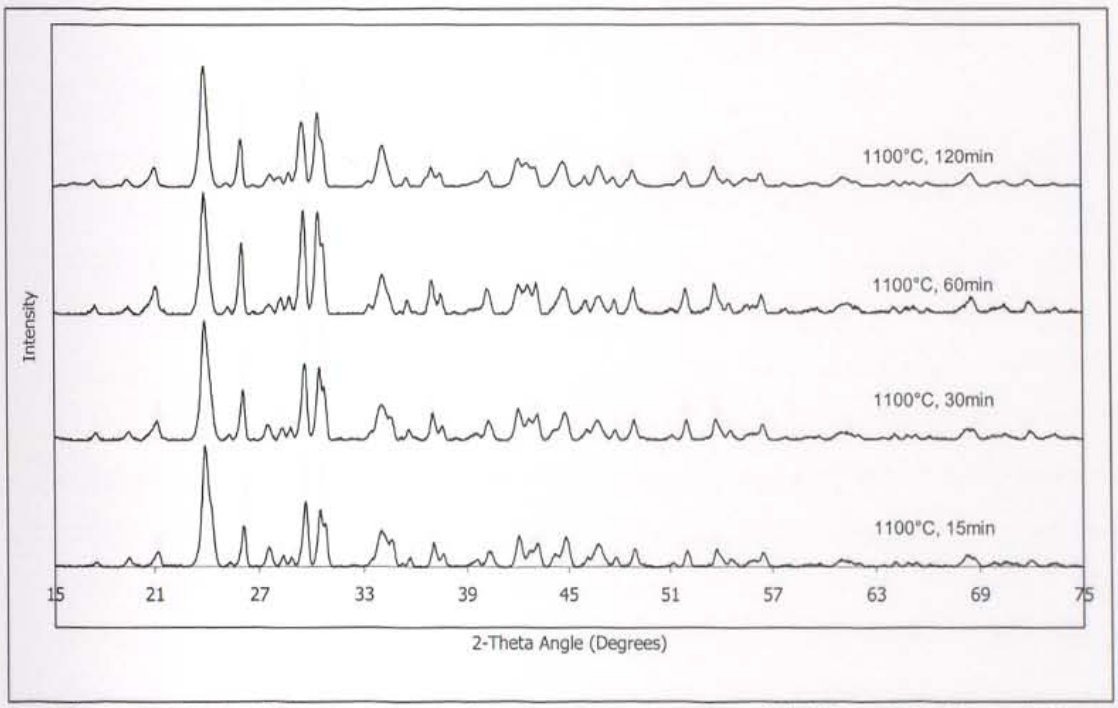

Figure 3.47: Diffractograms of quaternary samples with M_S = 2.3, M_A = 1.5 and BSF = 98 %, heated at 900 °C for 60 minutes and then at 1100 °C for different time periods

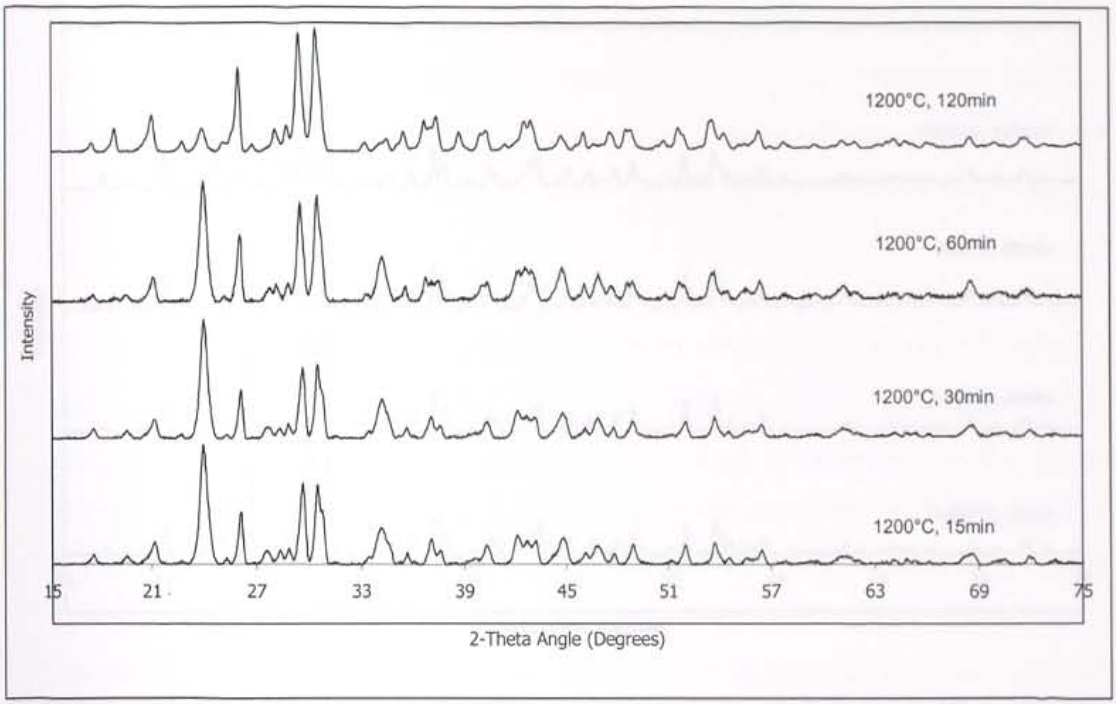

Figure 3.48: Diffractograms of quaternary samples with M_S = 2.3, M_A = 1.5 and BSF = 98 %, heated at 900 °C for 60 minutes and then at 1200 °C for different time periods

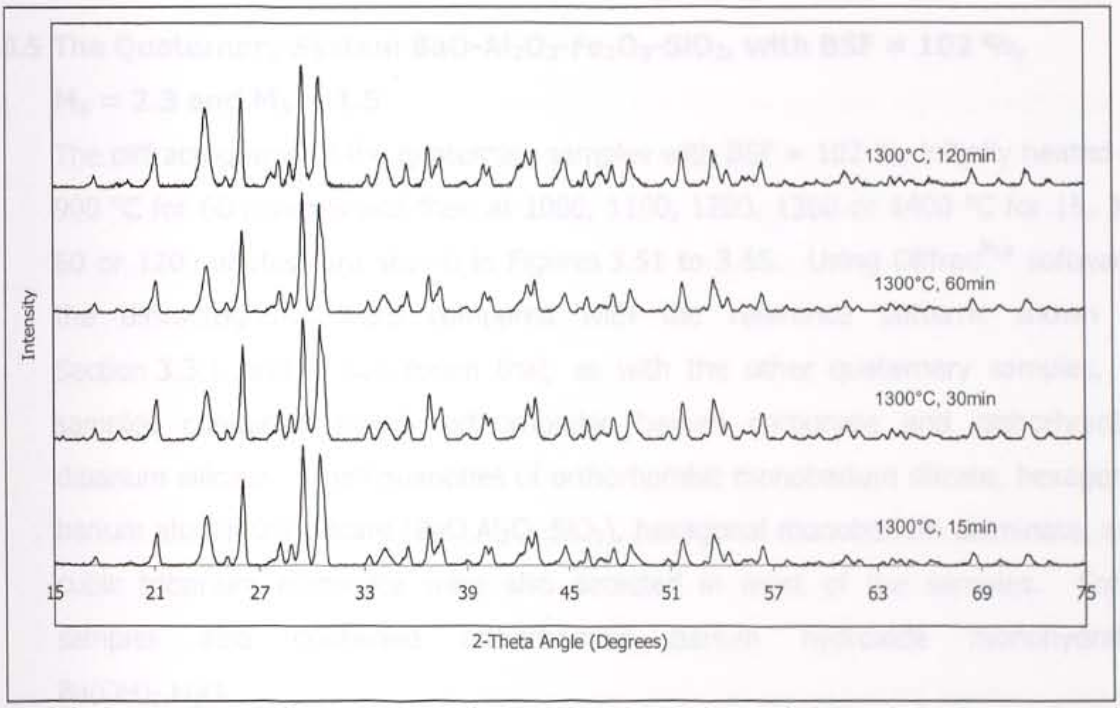

Figure 3.49: Diffractograms of quaternary samples with M_S = 2.3, M_A = 1.5 and BSF = 98 %, heated at 900 °C for 60 minutes and then at 1300 °C for different time periods

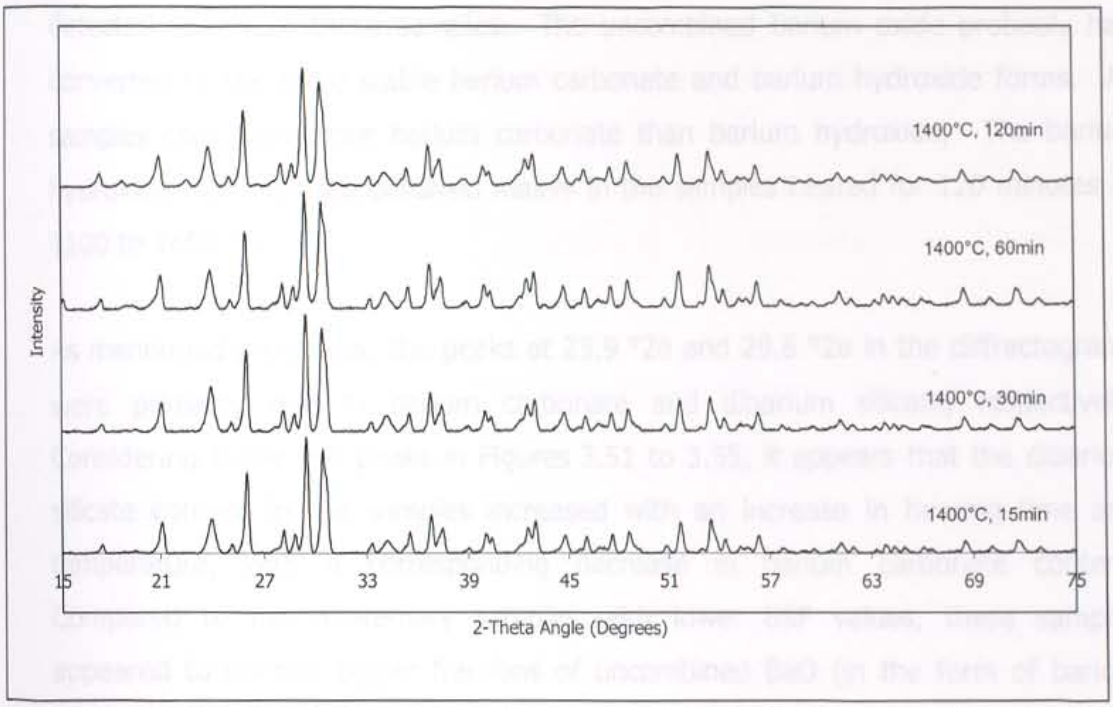

Figure 3.50: Diffractograms of quaternary samples with M_S = 2.3, M_A = 1.5 and BSF = 98 %, heated at 900 °C for 60 minutes and then at 1400 °C for different time periods

3.6.5 The Quaternary System $BaO-Al_2O_3-Fe_2O_3-SiO_2$, with BSF = 102 %, M_S = 2.3 and M_A = 1.5

The diffractograms of the quaternary samples with BSF = 102 %, initially heated at 900 °C for 60 minutes and then at 1000, 1100, 1200, 1300 or 1400 °C for 15, 30, 60 or 120 minutes, are shown in Figures 3.51 to 3.55. Using Diffrac^{Plus} software, the diffractograms were compared with the reference patterns shown in Section 3.3.1 and it was found that, as with the other quaternary samples, all samples contained mainly orthorhombic barium carbonate and orthorhombic dibarium silicate. Small quantities of orthorhombic monobarium silicate, hexagonal barium aluminium silicate ($BaO.Al_2O_3.SiO_2$), hexagonal monobarium aluminate, and cubic tribarium aluminate were also detected in most of the samples. Some samples also contained orthorhombic barium hydroxide monohydrate, $Ba(OH)_2.H_2O$.

Similarly to the other quaternary samples, no uncombined barium oxide was

detected in any of these samples. The uncombined barium oxide probably had converted to the more stable barium carbonate and barium hydroxide forms. All samples contained more barium carbonate than barium hydroxide. The barium hydroxide monohydrate occurred mainly in the samples heated for 120 minutes at 1100 to 1400 °C.

As mentioned previously, the peaks at 23.9 °2θ and 29.6 °2θ in the diffractograms were primarily due to barium carbonate and dibarium silicate, respectively. Considering these two peaks in Figures 3.51 to 3.55, it appears that the dibarium silicate content in the samples increased with an increase in heating time and temperature, with a corresponding decrease in barium carbonate content. Compared to the quaternary samples with lower BSF values, these samples appeared to contain bigger fractions of uncombined BaO (in the form of barium carbonate) at a specific temperature.

Monobarium silicate was present in various samples in the temperature range 1000 to 1400 °C, but no particular trend could be observed.

Barium aluminium silicate was detected in the sample heated for 120 minutes at 1100 °C and in all samples heated in the temperature range 1200 to 1400 °C. Monobarium aluminate was only present in samples heated for up to 60 minutes in the temperature range 1100 to 1300 °C. Tribarium aluminate was present in all samples heated in the temperature range 1000 to 1400 °C.

The crystalline phases identified in the samples with BSF = 102 %, are listed in Tables 3.28 to 3.32. Descriptions of these phases are given in Table 3.2 and Appendix A. The distinction between major and minor phases in the tables depended on the relative peak intensities of the individual phases in the diffractograms. The peaks in the diffractograms due to the minor phases were, in general, too small to observe any trends of these phases with heating time or temperature.

Table 3.28: Crystalline phases identified in samples with M_S = 2.3, M_A = 1.5 and BSF = 102 %, heated at 900 °C for 60 minutes and then at 1000 °C for different time periods

BSF (%)	Temperature (°C)	Heating Time (minutes)	Major Phase(s)	Minor Phase(s)
102	1000	15	$BaCO_3$ $2BaO.SiO_2$	$BaO.SiO_2$ $3BaO.Al_2O_3$
102	1000	30	$BaCO_3$ $2BaO.SiO_2$	$3BaO.Al_2O_3$
102	1000	60	$BaCO_3$ $2BaO.SiO_2$	$3BaO.Al_2O_3$
102	1000	120	$BaCO_3$ $2BaO.SiO_2$	$3BaO.Al_2O_3$

Table 3.29: Crystalline phases identified in samples with M_S = 2.3, M_A = 1.5 and BSF = 102 %, heated at 900 °C for 60 minutes and then at 1100 °C for different time periods

BSF (%)	Temperature (°C)	Heating Time (minutes)	Major Phase(s)	Minor Phase(s)
102	1100	15	$BaCO_3$ $2BaO.SiO_2$	$BaO.SiO_2$ $BaO.Al_2O_3$ $3BaO.Al_2O_3$
102	1100	30	$BaCO_3$ $2BaO.SiO_2$	$BaO.SiO_2$ $BaO.Al_2O_3$ $3BaO.Al_2O_3$
102	1100	60	$BaCO_3$ $2BaO.SiO_2$	$BaO.Al_2O_3$ $3BaO.Al_2O_3$
102	1100	120	$BaCO_3$ $2BaO.SiO_2$	$BaO.Al_2O_3.SiO_2$ $3BaO.Al_2O_3$ $Ba(OH)_2.H_2O$

Table 3.30: Crystalline phases identified in samples with M_S = 2.3, M_A = 1.5 and BSF = 102 %, heated at 900 °C for 60 minutes and then at 1200 °C for different time periods

BSF (%)	Temperature (°C)	Heating Time (minutes)	Major Phase(s)	Minor Phase(s)
102	1200	15	$BaCO_3$ $2BaO.SiO_2$	$BaO.SiO_2$ $BaO.Al_2O_3.SiO_2$ $BaO.Al_2O_3$ $3BaO.Al_2O_3$
102	1200	30	$BaCO_3$ $2BaO.SiO_2$	$BaO.SiO_2$ $BaO.Al_2O_3.SiO_2$ $BaO.Al_2O_3$ $3BaO.Al_2O_3$
102	1200	60	$BaCO_3$ $2BaO.SiO_2$	$BaO.SiO_2$ $BaO.Al_2O_3.SiO_2$ $BaO.Al_2O_3$ $3BaO.Al_2O_3$ $Ba(OH)_2.H_2O$
102	1200	120	$BaCO_3$ $2BaO.SiO_2$	$BaO.SiO_2$ $BaO.Al_2O_3.SiO_2$ $3BaO.Al_2O_3$ $Ba(OH)_2.H_2O$

Table 3.31: Crystalline phases identified in samples with M_S = 2.3, M_A = 1.5 and BSF = 102 %, heated at 900 °C for 60 minutes and then at 1300 °C for different time periods

BSF (%)	Temperature (°C)	Heating Time (minutes)	Major Phase(s)	Minor Phase(s)
102	1300	15	$BaCO_3$ $2BaO.SiO_2$	$BaO.SiO_2$ $BaO.Al_2O_3.SiO_2$ $BaO.Al_2O_3$ $3BaO.Al_2O_3$
102	1300	30	$BaCO_3$ $2BaO.SiO_2$	$BaO.SiO_2$ $BaO.Al_2O_3.SiO_2$ $BaO.Al_2O_3$ $3BaO.Al_2O_3$
102	1300	60	$BaCO_3$ $2BaO.SiO_2$	$BaO.Al_2O_3.SiO_2$ $BaO.Al_2O_3$ $3BaO.Al_2O_3$
102	1300	120	$BaCO_3$ $2BaO.SiO_2$	$BaO.Al_2O_3.SiO_2$ $3BaO.Al_2O_3$ $Ba(OH)_2.H_2O$

Table 3.32: Crystalline phases identified in samples with M_S = 2.3, M_A = 1.5 and BSF = 102 %, heated at 900 °C for 60 minutes and then at 1400 °C for different time periods

BSF (%)	Temperature (°C)	Heating Time (minutes)	Major Phase(s)	Minor Phase(s)
102	1400	15	$BaCO_3$ $2BaO.SiO_2$	$BaO.SiO_2$ $BaO.Al_2O_3.SiO_2$ $3BaO.Al_2O_3$
102	1400	30	$BaCO_3$ $2BaO.SiO_2$	$BaO.SiO_2$ $BaO.Al_2O_3.SiO_2$ $3BaO.Al_2O_3$
102	1400	60	$BaCO_3$ $2BaO.SiO_2$	$BaO.SiO_2$ $BaO.Al_2O_3.SiO_2$ $3BaO.Al_2O_3$
102	1400	120	$BaCO_3$ $2BaO.SiO_2$	$BaO.SiO_2$ $BaO.Al_2O_3.SiO_2$ $3BaO.Al_2O_3$ $Ba(OH)_2.H_2O$

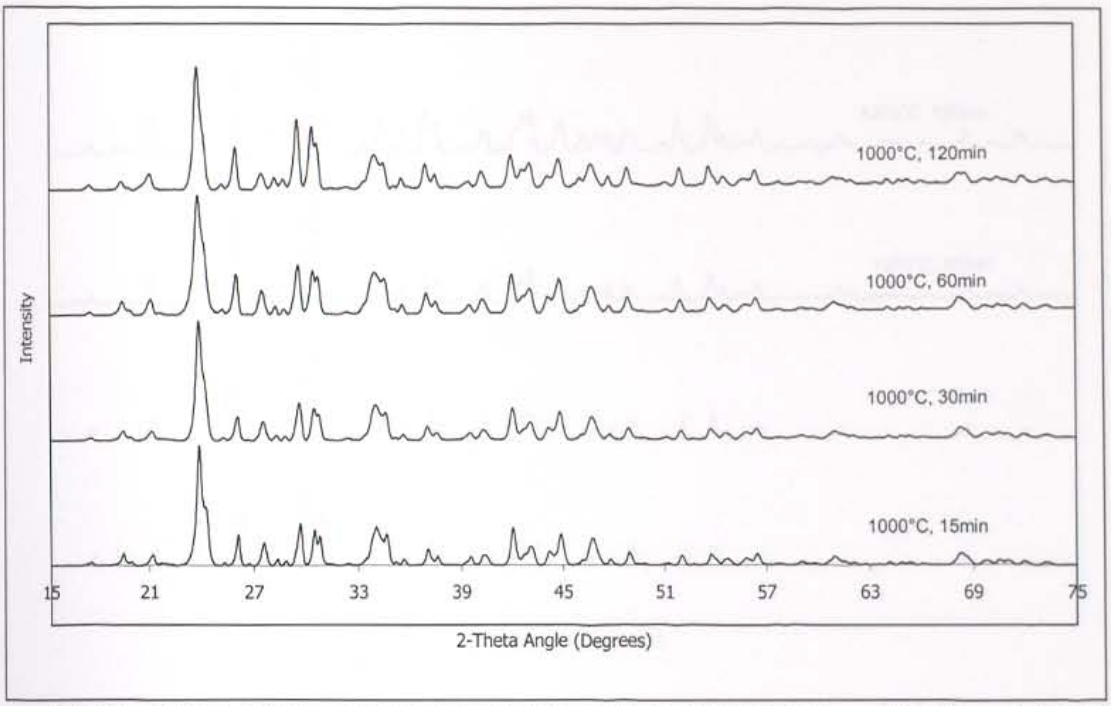

Figure 3.51: Diffractograms of quaternary samples with M_S = 2.3, M_A = 1.5 and BSF = 102 %, heated at 900 °C for 60 minutes and then at 1000 °C for different time periods

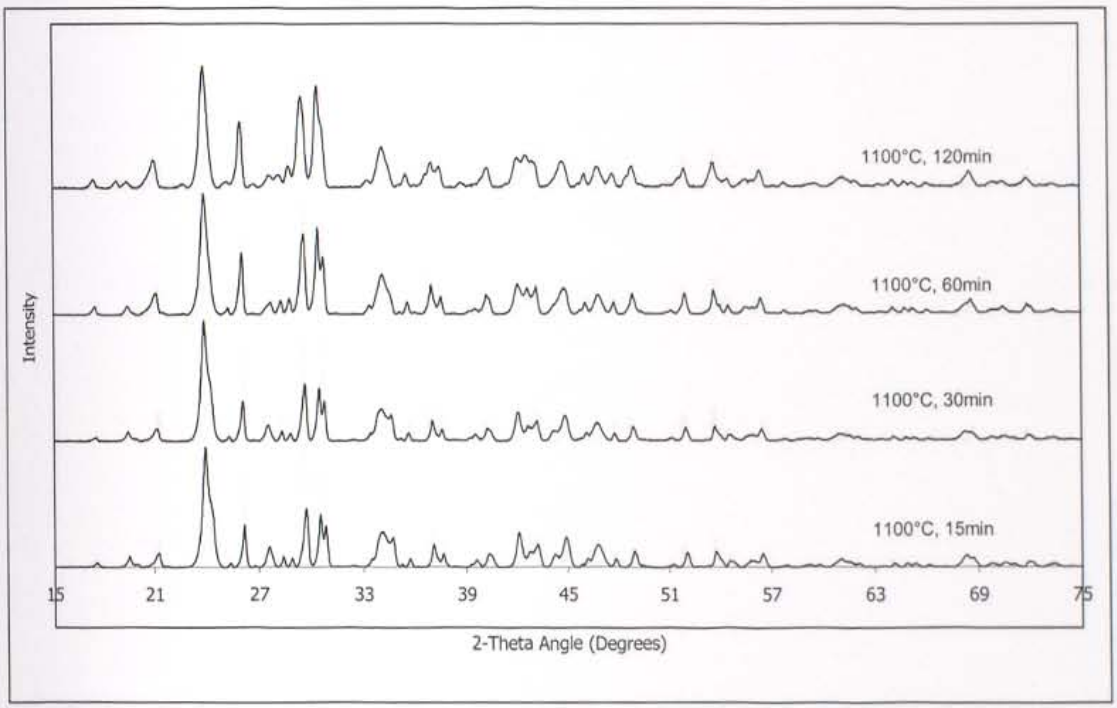

Figure 3.52: Diffractograms of quaternary samples with M_S = 2.3, M_A = 1.5 and BSF = 102 %, heated at 900 °C for 60 minutes and then at 1100 °C for different time periods

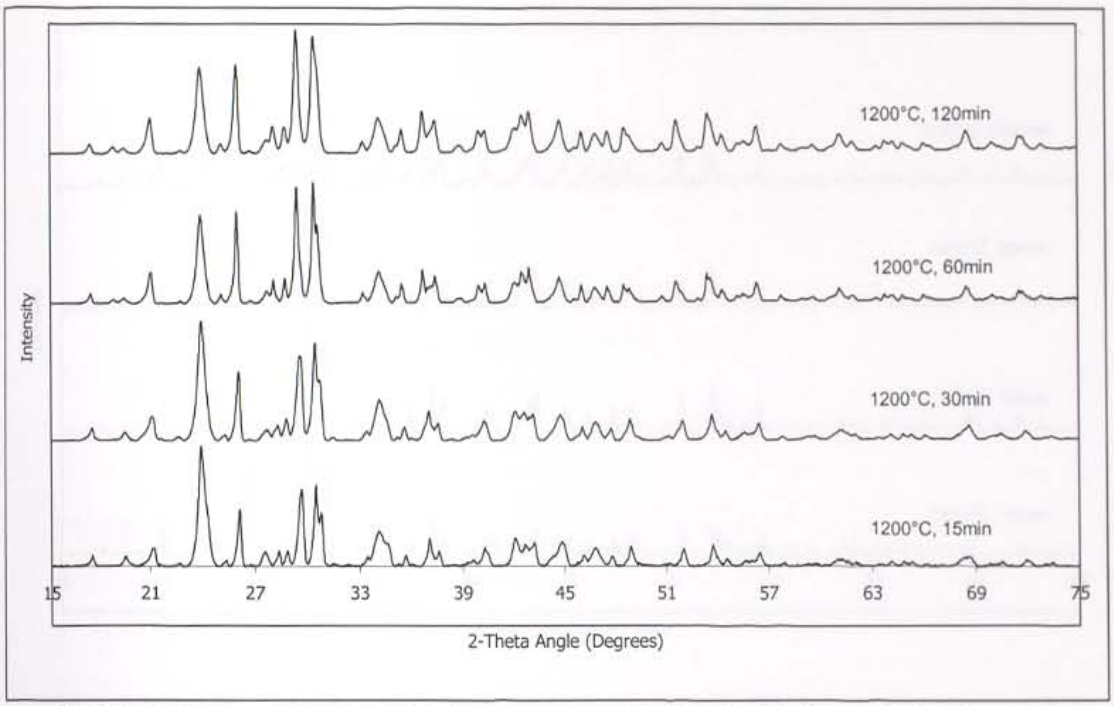

Figure 3.53: Diffractograms of quaternary samples with M_S = 2.3, M_A = 1.5 and BSF = 102 %, heated at 900 °C for 60 minutes and then at 1200 °C for different time periods

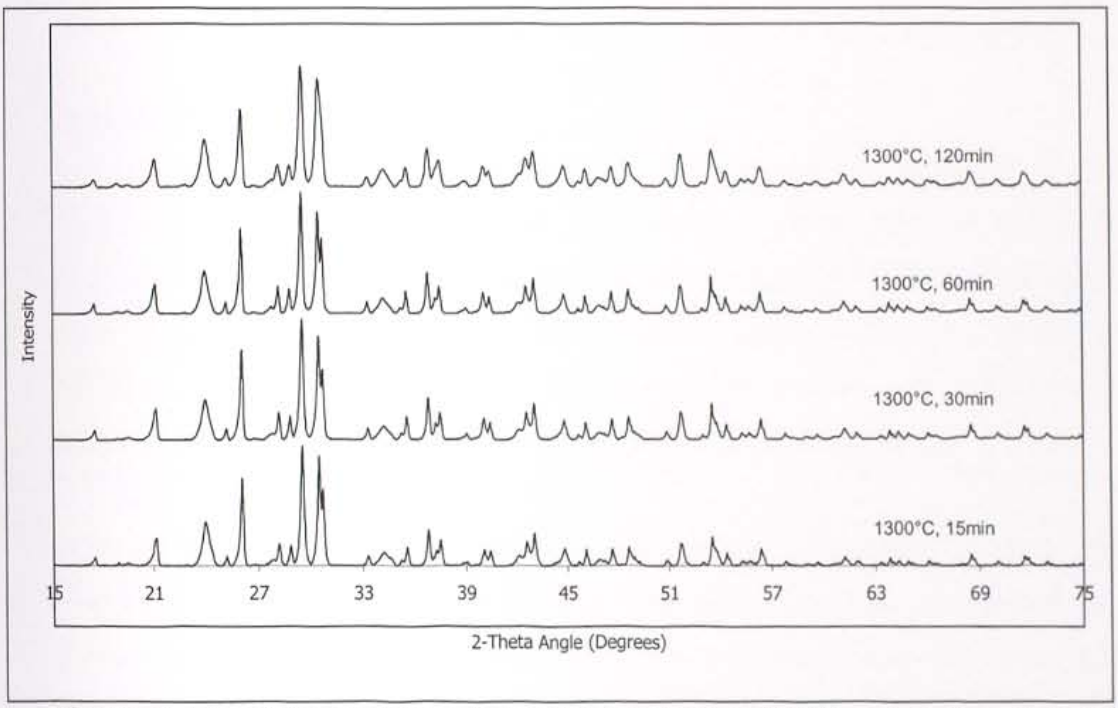

Figure 3.54: Diffractograms of quaternary samples with M_S = 2.3, M_A = 1.5 and BSF = 102 %, heated at 900 °C for 60 minutes and then at 1300 °C for different time periods

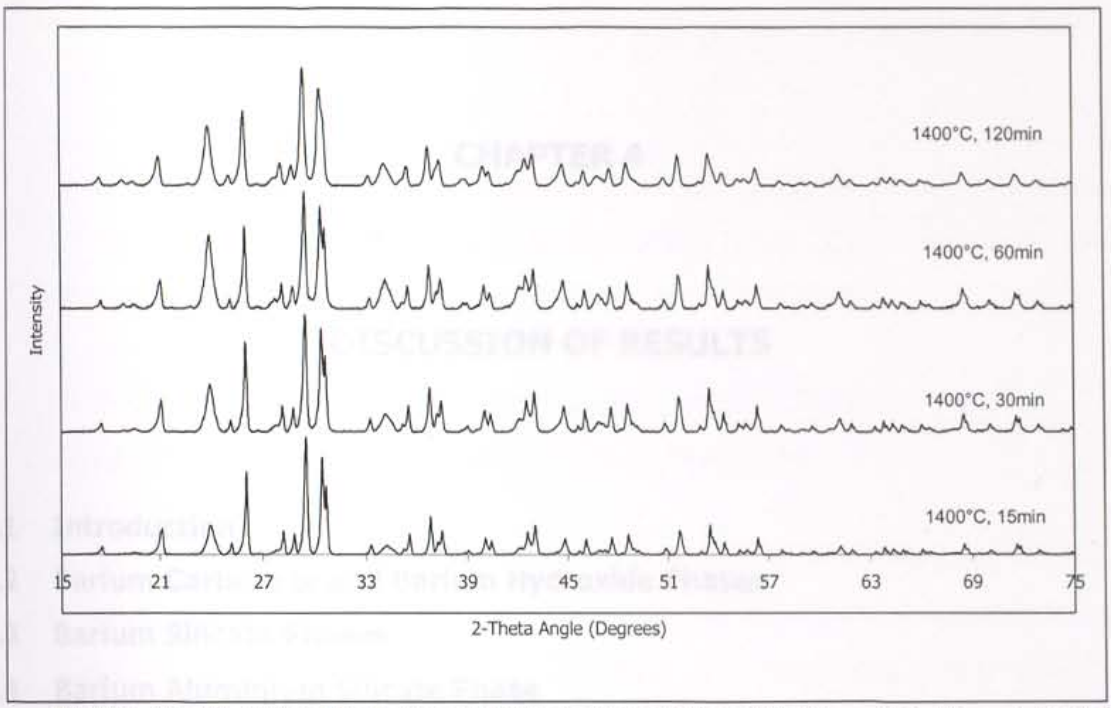

Figure 3.55: Diffractograms of quaternary samples with M_S = 2.3, M_A = 1.5 and BSF = 102 %, heated at 900 °C for 60 minutes and then at 1400 °C for different time periods